Proteomic Dissection of the Impact of Environmental Exposures on Mouse Seminal Vesicle Function

Authors

David A. Skerrett-Byrne, Natalie A. Trigg, Elizabeth G. Bromfield, Matthew D. Dun, Ilana R. Bernstein, Amanda L. Anderson, Simone J. Stanger, Lily A. MacDougall, Tessa Lord, R. John Aitken, Shaun D. Roman, Sarah A. Robertson, Brett Nixon, and John E. Schjenken

Correspondence

john.schjenken@newcastle.edu.au

In Brief

Seminal vesicles produce bioactive constituents that support gamete function and promote reproductive success. Despite their significance, seminal vesicle biology remains poorly defined. Here, we have exploited proteomics to generate the first mechanistic insights into mouse seminal vesicles in normal physiology and pathology. Our collective data affirm the hypothesis that seminal vesicles are sensitive to environmental factors and exposures in a manner that may have consequences for fetal development and later offspring health.

Graphical Abstract

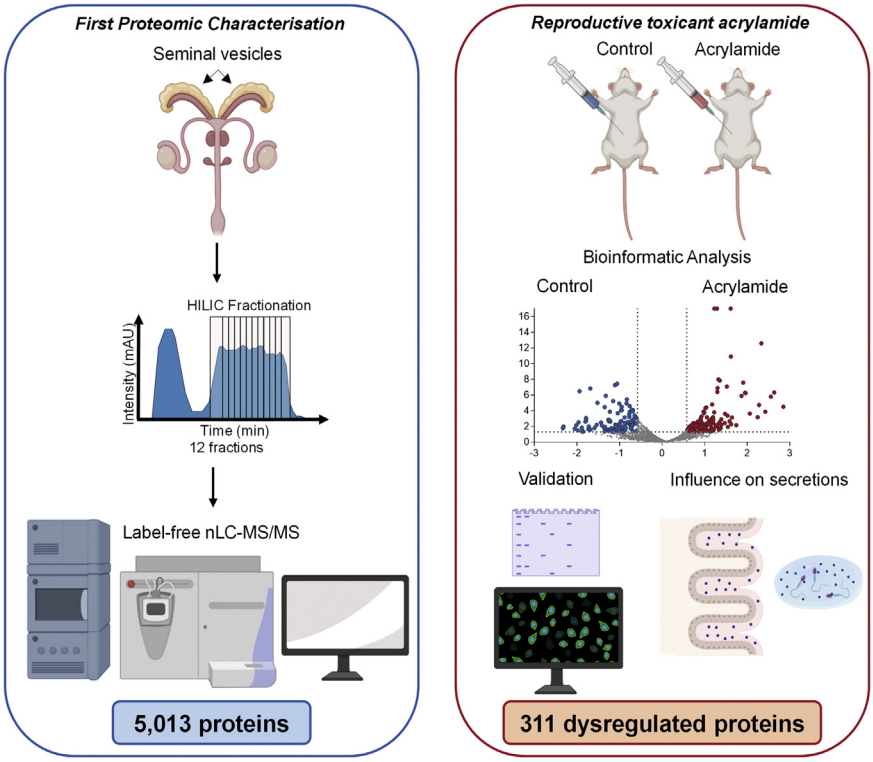

Highlights

- First proteomic characterization of the mouse seminal vesicle tissue.
- Secreted proteins are among the most abundant proteins in the seminal vesicle tissue.
- Paternal exposure to reproductive toxicant acrylamide alters seminal vesicle proteome.
- Acrylamide treatment results in reduced seminal vesicle secretory capacity.

2021, Mol Cell Proteomics *20*, 100107

https://doi.org/10.1016/j.mcpro.2021.100107

Proteomic Dissection of the Impact of Environmental Exposures on Mouse Seminal Vesicle Function

David A. Skerrett-Byrne[1,2], Natalie A. Trigg[1,2], Elizabeth G. Bromfield[1,2,3], Matthew D. Dun[4,5], Ilana R. Bernstein[1,2], Amanda L. Anderson[1,2], Simone J. Stanger[1,2], Lily A. MacDougall[1,2], Tessa Lord[1,2], R. John Aitken[1,2], Shaun D. Roman[1,2], Sarah A. Robertson[6], Brett Nixon[1,2,‡], and John E. Schjenken[1,2,*‡]

Seminal vesicles are an integral part of the male reproductive accessory gland system. They produce a complex array of secretions containing bioactive constituents that support gamete function and promote reproductive success, with emerging evidence suggesting these secretions are influenced by our environment. Despite their significance, the biology of seminal vesicles remains poorly defined. Here, we complete the first proteomic assessment of mouse seminal vesicles and assess the impact of the reproductive toxicant acrylamide. Mice were administered acrylamide (25 mg/kg bw/day) or control daily for five consecutive days prior to collecting seminal vesicle tissue. A total of 5013 proteins were identified in the seminal vesicle proteome with bioinformatic analyses identifying cell proliferation, protein synthesis, cellular death, and survival pathways as prominent biological processes. Secreted proteins were among the most abundant, and several proteins are linked with seminal vesicle phenotypes. Analysis of the effect of acrylamide on the seminal vesicle proteome revealed 311 differentially regulated (FC ± 1.5, $p \leq 0.05$, 205 up-regulated, 106 downregulated) proteins, orthogonally validated *via* immunoblotting and immunohistochemistry. Pathways that initiate protein synthesis to promote cellular survival were prominent among the dysregulated pathways, and rapamycin-insensitive companion of mTOR (RICTOR, $p = 6.69E-07$) was a top-ranked upstream driver. Oxidative stress was implicated as contributing to protein changes, with acrylamide causing an increase in 8-OHdG in seminal vesicle epithelial cells (fivefold increase, $p = 0.016$) and the surrounding smooth muscle layer (twofold increase, $p = 0.043$). Additionally, acrylamide treatment caused a reduction in seminal vesicle secretion weight (36% reduction, $p = 0.009$) and total protein content (25% reduction, $p = 0.017$). Together these findings support the interpretation that toxicant exposure influences male accessory gland physiology and highlights the need to consider the response of all male reproductive tract tissues when interpreting the impact of environmental stressors on male reproductive function.

The male accessory sex glands comprise the prostate, seminal vesicles, and bulbourethral glands (1). The combined secretory activity of these tissues gives rise to seminal plasma, a highly viscous fluid containing a complex array of bioactive molecules that support male gamete function after ejaculation and stimulate gene expression and immune response changes in the female reproductive tract (2, 3). In the majority of mammalian species, including humans, the androgen-dependent seminal vesicles are the dominant contributor to seminal plasma (4, 5). Indeed, elegant experiments to surgically excise the accessory glands have clearly established seminal vesicles as being the most influential tissue that contributes to the rodent ejaculate. In rodents, seminal vesicle secretions are directly implicated in regulating the conception environment within the female reproductive tract to elicit an immune response that promotes optimal fetal development and supports long-term offspring health (1, 2, 4, 6–11). In view of the mounting evidence that such roles are conserved among mammals (12–14), it is likely that the

From the [1]Priority Research Centre for Reproductive Science, School of Environmental and Life Sciences, Discipline of Biological Sciences, The University of Newcastle, Callaghan, NSW, Australia; [2]Pregnancy and Reproduction Program, Hunter Medical Research Institute, New Lambton Heights, NSW, Australia; [3]Department of Biochemistry and Cell Biology, Faculty of Veterinary Medicine, Utrecht University, Utrecht, The Netherlands; [4]Cancer Signalling Research Group, Faculty of Health and Medicine, School of Biomedical Sciences and Pharmacy, University of Newcastle, Callaghan, NSW, Australia; [5]Priority Research Centre for Cancer Research Innovation and Translation, Hunter Medical Research Institute, Lambton, NSW, Australia; [6]The Robinson Research Institute and Adelaide Medical School, University of Adelaide, Adelaide, SA, Australia

‡These authors contributed equally to this work.

*For correspondence: John Schjenken, john.schjenken@newcastle.edu.au.

https://doi.org/10.1016/j.mcpro.2021.100107

complex molecular signals contained within seminal plasma are of critical importance for promoting reproductive success and maximizing progeny fitness.

The regulatory influence exerted by seminal vesicle secretions at conception (1) provides impetus to understand whether this tissue is affected by lifestyle and/or environmental exposures (3, 15). While genetic and epigenetic alterations to the male germline are conventionally thought to account for the transmission of paternal environmental exposures to subsequent generations, emerging evidence demonstrates that altered function of seminal vesicle tissue may exert an important influential role (3, 16, 17). An impact of the paternal environment on seminal vesicle function has been observed in rams, where seminal vesicle proteins were altered in response to paternal heat stress (18), while neonatal exposure to the endocrine-disrupting compound, diethylstilbestrol, leads to toxicity in mouse seminal vesicle from early developmental stages (19). Compelling data comes from rodent models, where paternal diet has been demonstrated to shape offspring health through mechanisms involving both the fertilizing spermatozoon and the seminal plasma in which they are delivered (16, 20). Together, these data highlight that altered seminal vesicle fluid composition not only has potential to impair fertility but may also affect fetal development and impart long-term health consequences for offspring (3, 16, 17, 21).

To develop an understanding of the impact of environmental exposures on male reproductive function, we have previously used acrylamide as a reproductive toxicant to assess its impact on germ cell populations in the testes and in epididymis (22–24). In these former studies, we demonstrated that acrylamide exposure leads to elevated levels of DNA damage throughout sperm development and maturation, with subtle changes in Sertoli cell structure following long-term acrylamide exposure. Specifically, exposure of testicular germ cells to acrylamide leads to enhanced levels of DNA damage that fail to be resolved during sperm maturation, yet do not appear to affect fertility or fetal development. Comparable levels of DNA damage are also characteristic of sperm exclusively exposed to acrylamide during epididymal transit. However, exposure timed to coincide with the developmental window of epididymal transit and ejaculation leads to substantially increased rates of fetal loss. These data indicate that the male transfers the burden of acrylamide stress to the female through mechanisms that are independent of sperm DNA damage. These results gave us the impetus to utilize this acute exposure model to assess acrylamide impact on the seminal vesicles, to better understand the contribution of this understudied tissue to a male's response to reproductive insults.

To begin to address this challenge, we have completed the first proteomic assessment of mouse seminal vesicle tissues using offline peptide fractionation *via* hydrophilic interaction liquid chromatography coupled with high-resolution reverse-phase nanoflow liquid chromatography–tandem mass spectrometry (nLC-MS/MS). Additionally, we have exploited an established model involving acute exposure to the reproductive toxicant acrylamide that we have previously demonstrated alters male gamete quality and increases fetal loss (22), to explore the impact of this environmental exposure on seminal vesicle function. The results highlight cellular mechanisms altered in the seminal vesicles in response to acrylamide and thus provide evidence that this crucial reproductive tissue is sensitive to environmental factors and exposures.

EXPERIMENTAL PROCEDURES

Ethics Approval

All experimental procedures involving mice were conducted with the approval of the University of Newcastle Animal Care and Ethics Committee (approval number A-2017-726). Male outbred Swiss mice (8–12 weeks of age) were obtained from a breeding colony held at the University of Newcastle central animal facility and maintained according to the recommendations prescribed by the Animal Care and Ethics Committee. Mice were housed under a controlled lighting regimen (12-h light: 12 h dark) at 21 to 22 °C and supplied with food and water *ad libitum*.

Chemicals and Reagents

All reagents were purchased from Merck, unless otherwise specified.

Acrylamide Treatment Regimen and Tissue Collection

Mice received an intraperitoneal injection of acrylamide (25 mg/kg bw/day) or control (phosphate buffered saline (PBS): 0.01 M phosphate buffer, 0.0027 M KCl and 0.137 M NaCl, pH 7.4) each morning for five consecutive days (injection volume 100 μl) according to an established acute exposure protocol described in Katen *et al.* (22), which results in fetal loss in females sired by acrylamide-treated males. In accordance with this established exposure regimen, mice were euthanized 72 h following the final acrylamide injection, and seminal vesicles were dissected and weighed, ensuring that the anterior prostate (coagulating gland) was left *in situ*. Seminal vesicle fluid was expelled from one gland by gently squeezing seminal vesicle tissue using forceps and then weighed. Tissues were washed thoroughly in Tris-buffered saline (TBS) comprising 50 mM Tris-HCl, 150 mM NaCl, in mass spectrometry grade H_2O, pH 7.6. In separate tubes, tissue and fluid were snap frozen in liquid nitrogen and stored at −80 °C. For histological analysis, excised seminal vesicles from the gland containing seminal vesicle fluid were fixed for 8 h in Bouin's solution (5% v/v acetic acid, 25% v/v formaldehyde, 70% v/v picric acid). Bouin's solution was removed with daily changes of 75% (v/v) ethanol for at least 5 days. Tissues were embedded in paraffin and 5 μm sections were cut prior to staining with hematoxylin and eosin. Stained sections were examined and photographed on a Zeiss Axio A.2 fluorescence microscope (Carl Zeiss AG) and epithelial cell height and epithelial mucosal folding assessed using OLYMPUS cellSens standard software (Olympus Corporation), as described (25).

Proteomic Sample Preparation of Mouse Seminal Vesicles

Seminal vesicle tissues were cut into small segments with a scalpel and homogenized in ice-cold 0.1 M Na_2CO_3 containing protease and complete EDTA-free phosphatase inhibitors (Roche Holding AG) using a FastPrep-24TM 5G homogenizer (MP Biomedicals) with a Cool Prep

Adaptor (2 × 1 min, 4.0 m/s, at 4 °C). Homogenized samples were then sonicated (3 × 10 s cycles, 100% output power). Protein concentration was determined using a bicinchoninic acid assay (Thermo Fisher Scientific) and diluted to a final concentration of 1.4 mg in a solution of 6 M urea and 2 M thiourea. Samples underwent reduction and alkylation with 10 mM dithiothreitol (30 min at room temperature) and 20 mM iodoacetamide (30 min protected from light at room temperature) respectively. Peptide populations were digested with 1:30 Lys-C/Trypsin Mix (Promega) (26–30) at room temperature for 3 h. Using 50 mM triethylammonium bicarbonate, the concentration of urea was brought below 1 M and digested overnight at 37 °C. Lipids were precipitated from peptide suspensions using formic acid (2% v/v final concentration), and the resultant peptides were purified using Oasis 1 cc desalting columns (Waters Corp). Peptides were quantified using the Qubit protein assay (Thermo Fisher Scientific), and 48 μg of each sample was subjected to offline fractionation *via* hydrophilic interaction liquid chromatography (HILIC) (Fig. 1, supplemental Fig. S1, *A* and *B*).

nLC-MS/MS Analysis

Reverse-phase nLC-MS/MS was performed on control and acrylamide-treated HILIC fractions (12 from each seminal vesicle) (supplemental Fig. S1, *A* and *B*) using a Q-Exactive Plus hybrid quadrupole-Orbitrap MS coupled to a Dionex Ultimate 3000RSLC nanoflow high-performance LC system (Thermo Fisher Scientific). Samples were loaded onto an Acclaim PepMap 100 C18 75 μm × 20 mm trap column (Thermo Fisher Scientific) for preconcentration and online desalting. Separation was then achieved using an EASY-Spray PepMap C18 75 μm × 250 mm column (Thermo Fisher Scientific), employing a linear gradient of acetonitrile (2–40%, 300 nl/min, 120 min). The MS was operated in data-dependent acquisition (DDA) mode. The Orbitrap mass analyzer was used at a resolution of 35,000, to acquire full MS with an m/z range of 380 to 2000, incorporating a target automatic gain control value of 1×10^6 and maximum fill times of 50 ms. The 20 most intense multiple charged precursors were selected for higher-energy collision dissociation fragmentation with stepped collisional energies of 25%, 28%, and 30%. MS/MS fragments were measured at an Orbitrap resolution of 17,500 using an automatic gain control target of 5×10^5 and maximum fill time of 120 ms.

Data Processing and Analysis

Database searching of all raw files was performed using Proteome Discoverer 2.4 (Thermo Fisher Scientific). SEQUEST HT was used to search against the UniProt *Mus musculus* database (25,260 sequences, downloaded November 12, 2019). Database searching parameters included up to two missed cleavages, a precursor mass tolerance set to 10 ppm, fragment mass tolerance of 0.02 Da, and trypsin designated as the digestion enzyme. Cysteine carbamidomethylation was set as a fixed modification while dynamic modifications included acetylation (N-terminus), oxidation (M), and phosphorylation (S/T and Y). Interrogation of the corresponding reversed database was also performed to evaluate the false discovery rate (FDR) of peptide identification using Percolator based on q-values, which were estimated from the target-decoy search approach. To filter out target peptide spectrum matches over the decoy-peptide spectrum matches, a fixed FDR of 1% was set at the peptide level. Mass recalibration and label-free quantification (LFQ) of area under the curve MS1 peaks were carried out using Proteome Discoverer nodes, Spectrum Files RC, Minora Feature Detector, and Feature Mapper (31–37). Minora Feature Detector is the dominant algorithm behind the LFQ whereby it first detects chromatographic peaks in the raw spectral data and maps them to identified peptide spectrum matches. A feature is created when a peak fits the mapping of chromatographic peaks to the calculated theoretical isotope patterns of the PSM. A similar process occurs for peaks that have no association with any features; this is calculated by accruing all chromatographic peaks within a short retention time range and searching for peaks that fit isotope patterning. To be accepted, intensities and mass deviations of these peaks must fit a theoretical pattern of an Averagine peptide. The Feature Mapper node builds on the Minora output and carries out a retention time alignment and feature/peptide linking within groups. Fold changes and significance between control and acrylamide-treated groups were calculated by Proteome Discoverer 2.4 using a nonnested pairwise ratio approach, whereby the program calculates the peptide group ratios as the geometric median of all combinations of ratios from all of the replicates for each group. Protein ratios were subsequently calculated as the geometric median of the peptide group ratios, and statistical testing was completed using a Student's *t* test. The protein list was exported as an Excel file and further refined to include only those with a quantitative value in all three replicates within at least one group (*i.e.*, control and/or acrylamide treated) and a minimum of two unique peptides. Using Perseus, version 1.6.10.43 (38), scatter plots of log-transformed normalized abundances (supplemental Fig. S1, *C* and *D*) were generated, and Pearson correlation (r2) was calculated, while global analysis of the data was undertaken to generate a principal component analysis plot. For a global illustration of protein abundance compared with fold-change, an MA plot was generated using Microsoft Excel. To determine the ranking order of proteins in the seminal vesicle tissue proteome by abundance, normalized abundance quants of the three biological replicates (prior to scaling) were averaged and ordered based on high to low.

Ingenuity Pathway Analysis

Ingenuity Pathway Analysis software (Qiagen) was used to analyze refined seminal vesicle tissue proteomic lists as previously described (26). Briefly, canonical pathways, upstream regulators, and disease and function analyses were generated and assessed by generating a *p*-value and Z-score enrichment measurement of the overlapping proteins from the dataset in a particular pathway, function, or regulator (39).

Phenotype and Seminal Vesicle Fluid Comparisons

The curated comparative proteome was searched against an exported protein list consisting of the full complement of Mouse Genome Informatics (40) and the International Mouse Phenotyping Consortium (41) datasets to identify those proteins expressed in the seminal vesicle that were also associated with seminal vesicle phenotypes. To further complement these analyses, proteomic datasets from three seminal vesicle fluid proteomic characterization papers (42–44) were obtained and filtered for reviewed proteins identified in UniProt. Proteins that were identified in at least one manuscript were then used to form a list of proteins expressed in mouse seminal vesicle fluid. This list was then compared with our seminal vesicle proteome.

Immunohistochemistry

Sections from Bouin's fixed seminal vesicle tissue were probed with antibodies using established methods for immunofluorescence and DAB immunohistochemistry analysis (22, 23, 27, 45). Sections were dewaxed in xylene and rehydrated. Antigen retrieval and blocking of nonspecific antibody binding were performed as described (supplemental Table S1). Sections were washed in PBS before incubation in primary antibodies (supplemental Table S1, in 1% w/v BSA diluted in PBS) overnight at 4 °C in a humidified chamber. Following washing in PBS (3 × 5 min), sections were incubated with appropriate secondary antibodies (supplemental Table S1, in 1% w/v BSA diluted in PBS) for 1 h at room temperature. Slides were washed in PBS (3 × 5 min) prior to mounting. For immunofluorescence analysis, slides

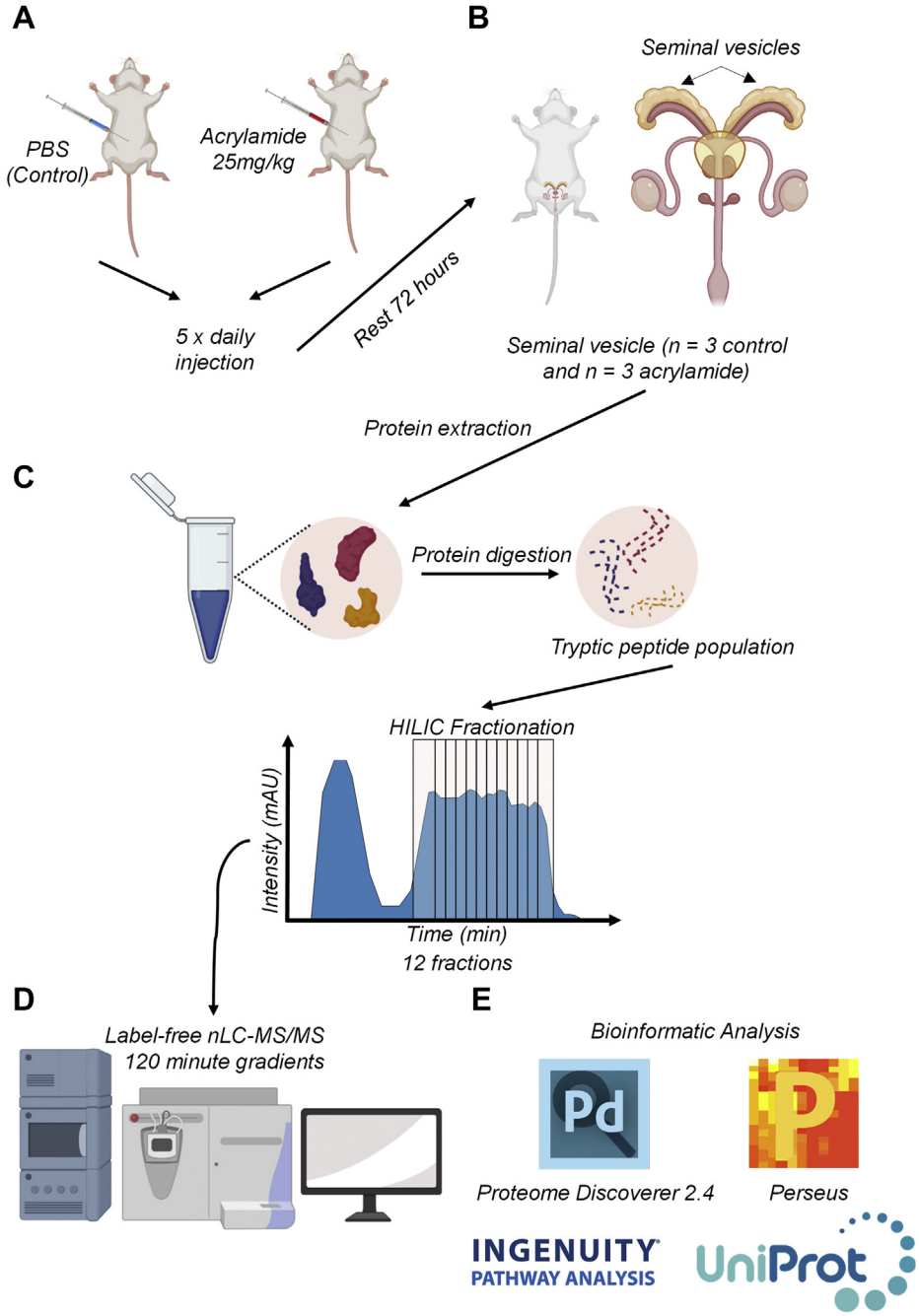

FIG. 1. **Overview of the proteomics workflow.** *A*, male Swiss mice (8–12 weeks of age, n = 3 per treatment group) were injected with acrylamide (25 mg/kg bw/day) or PBS (control) following the methods stated in Katen *et al.*, (22). *B*, following the final injection, mice were rested for 72 h prior to collection of seminal vesicles. *C*, protein was extracted, reduced, alkylated, and digested, prior to off-line fractionation of the tryptic peptide populations using hydrophilic interaction liquid chromatography (HILIC). *D*, HILIC fractions were then run on high-resolution nano liquid chromatography–tandem MS (nLC-MS/MS), before being, (*E*) analyzed with Proteome Discoverer 2.4, Perseus, Ingenuity Pathway Analysis, and UniProt. Some components of this figure created with BioRender.com.

were mounted in an antifade reagent comprising 10% v/v Mowiol 4 to 88, 30% v/v glycerol in 0.2 M Tris (pH 8.5), and 2.5% v/v 1,4-diazobicyclo-(2.2.2)-octane in 0.2 M Tris (pH 8.5). For immunohistochemistry analysis, detection was performed using diaminobenzidine tetrachloride, and sections were counterstained with hematoxylin and mounted in DPX mountant for histology. Slides were examined and photographed on a Zeiss Axio A.2 fluorescence microscope (Carl Zeiss AG). For 8-hydroxy-2'-deoxyguanosine (8-OHdG), ImageJ Fiji software (version 1.48v; National Institute of Health) (46, 47) was used to quantify the level of fluorescence normalized to DAPI labeling as described previously (23, 48). For alpha smooth muscle actin (αSMA) staining, OLYMPUS cellSens standard software (Olympus

Corporation) was used to assess the depth of the smooth muscle cell layer as described previously (25).

Sodium Dodecyl Sulfate–Polyacrylamide Gel Electrophoresis (SDS-PAGE) and Immunoblotting

Equivalent amounts of protein (10 μg) were boiled in SDS-PAGE sample buffer (2% v/v β2-mercaptoethanol, 2% w/v SDS, and 10% w/v sucrose in 0.375 M Tris, pH 6.8, with bromophenol blue) at 100 °C for 5 min, prior to being resolved by SDS-PAGE (150 V, 1 h), and transferred to nitrocellulose membranes (350 mA, 1 h). To detect proteins of interest, membranes were blocked under optimized conditions for 1 h at room temperature (Supplemental Table S1) before being incubated in primary antibody overnight at 4 °C (Supplemental Table S1). Following washing in (3 × 5 min in TBS supplemented with 0.1% (v/v) Tween-20 (TBST, pH 7.4)), sections were incubated with appropriate secondary antibodies for 1 h at room temperature. After additional washes (3 × 5 min in TBST), labeled proteins were detected using an enhanced chemiluminescence kit (GE Healthcare). For quantification of protein expression, relevant bands were assessed by densitometry using Multi Gauge V3.0 (Fujifilm) and normalized against glyceraldehyde-3-phosphate dehydrogenase. Data were expressed relative to the amount of protein in control seminal vesicle tissue.

Seminal Vesicle Fluid Solubilization and Quantification

Seminal vesicle fluid was collected and solubilized using a modified version of a previously reported method (49). Briefly, 8 M guanidine hydrochloride was added to seminal vesicle fluid and samples were vortexed for 5 min to completely dissolve the coagulated material. Immediately after, samples were incubated at 95 °C for 5 min to deactivate endogenous phosphatases and proteases and sonicated (3 × 10 s cycles, 100% output power). For protein quantification, samples were diluted to 2 M guanidine hydrochloride, and protein concentration was determined by a bicinchoninic acid assay (Thermo Fisher Scientific).

Experimental Design and Statistical Rationale

Proteomic analyses were performed using seminal vesicle tissue (n = 3 biological replicates collected from three individual mice/group). Differentially expressed proteins were defined as those with a fold-change ≥1.5 or ≤−1.5 and p value ≤0.05. All other data were assessed for normality using the Shapiro–Wilk normality test. Normally distributed data were analyzed by unpaired Student's t-tests to detect differences between treatment groups. Data not normally distributed were analyzed by a Mann–Whitney U test. Differences between groups were considered significant when $p \leq 0.05$. The number of biological replicates used in each experiment are presented in the figure captions. Graphical data were prepared using GraphPad Prism version 8.2.1 for Windows (GraphPad Software) and are presented as mean values ± SEM.

RESULTS

Analysis of the Global Mouse Seminal Vesicle Proteome

Secretions from the seminal vesicle exert substantial influence on male reproductive function (1, 2), but the biology of this tissue remains poorly defined. To address this, we have characterized the mouse seminal vesicle proteome using LFQ DDA high-resolution MS. Proteomic analysis of the control seminal vesicle tissue returned a complex core proteome comprising 5013 proteins ($FDR \leq 0.01$, Fig. 2*A*, supplemental Table S2) with high Pearson correlation coefficients (0.932 average r^2), across all biological replicates (supplemental Fig. S1*C*). An average of 16.4 peptides (14.9 unique peptides) were identified per seminal vesicle protein, representing a coverage of 39.8% per protein (Table 1). Further interrogation revealed that the majority (96.1%) of the proteome consists of known proteins with evidence at the protein level, but an additional 178 proteins (3.6%) had annotated evidence at the transcript level, and a further 15 proteins (0.3%) were identified that had only been inferred from homology (Fig. 2*B*, supplemental Table S2).

To gain an overview of the cellular localization and potential functions of the core seminal vesicle proteome, we utilized Ingenuity Pathway Analysis (39), which successfully mapped 4976/5013 (99.2%) of the identified proteome. Among the core seminal vesicle proteome, the majority of proteins were mapped to the cytoplasm (2861 proteins, 57.5%), followed by cellular localization within the nucleus (1108 proteins, 22.3%), plasma membrane (496 proteins, 10%), and extracellular space (306 proteins, 6.1%) (Fig. 2*C*), with the remaining 205 proteins (4.1%) mapped to the category "other." Classification of protein type revealed that the most common category of proteins were enzymes (1958 proteins, 39.3%), followed by transporters (373 proteins, 7.5%), transcription regulators (317 proteins, 6.6%), translation regulators (72 proteins, 1.4%), and receptors (63 proteins, 1.3%) (Fig. 2*D*). Proteins classified as ion channels, cytokines, and growth factors constituted less than 1% of the total proteome (Fig. 2*D*), while 2136 (42.9%) proteins were assigned to the functional category "other" (data not presented).

To assess the functional roles of proteins within the core mouse seminal vesicle proteome, Ingenuity Pathway Analysis was used to predict canonical pathways, downstream molecular, cellular, physiological system development, and disease functions associated with this proteome (Fig. 3, *A* and *B*, supplemental Tables S3 and S4). This strategy revealed that canonical pathways associated with cell proliferation, protein synthesis, and protein turnover were prominent (Fig. 3*A* and supplemental Table S3). Specifically, these signaling pathways included eukaryotic initiation factor (EIF)2 (cell proliferation and protein synthesis: 144 proteins, 70.2% coverage), regulation of EIF4 and P70S6K (cell proliferation and protein synthesis: 106 proteins, 71.6% coverage), protein ubiquitination (protein synthesis and protein turnover: 147 proteins, 56.1% coverage), and mTOR (cell proliferation, protein synthesis, and protein turnover: 120 proteins, 60.6% coverage). Among other relevant predicted pathways identified were cellular stress pathways, including mitochondrial dysfunction (120 proteins, 75% coverage), sirtuin signaling (158 proteins, 59% coverage), and nuclear factor erythroid 2-related factor-2 (NRF2)-mediated oxidative stress response (103 proteins, 57.5% coverage) (Fig. 3*A* and supplemental Table S3). Functions associated with both cell proliferation/protein production and cellular stress were also observed following assessment of molecular and physiological functions

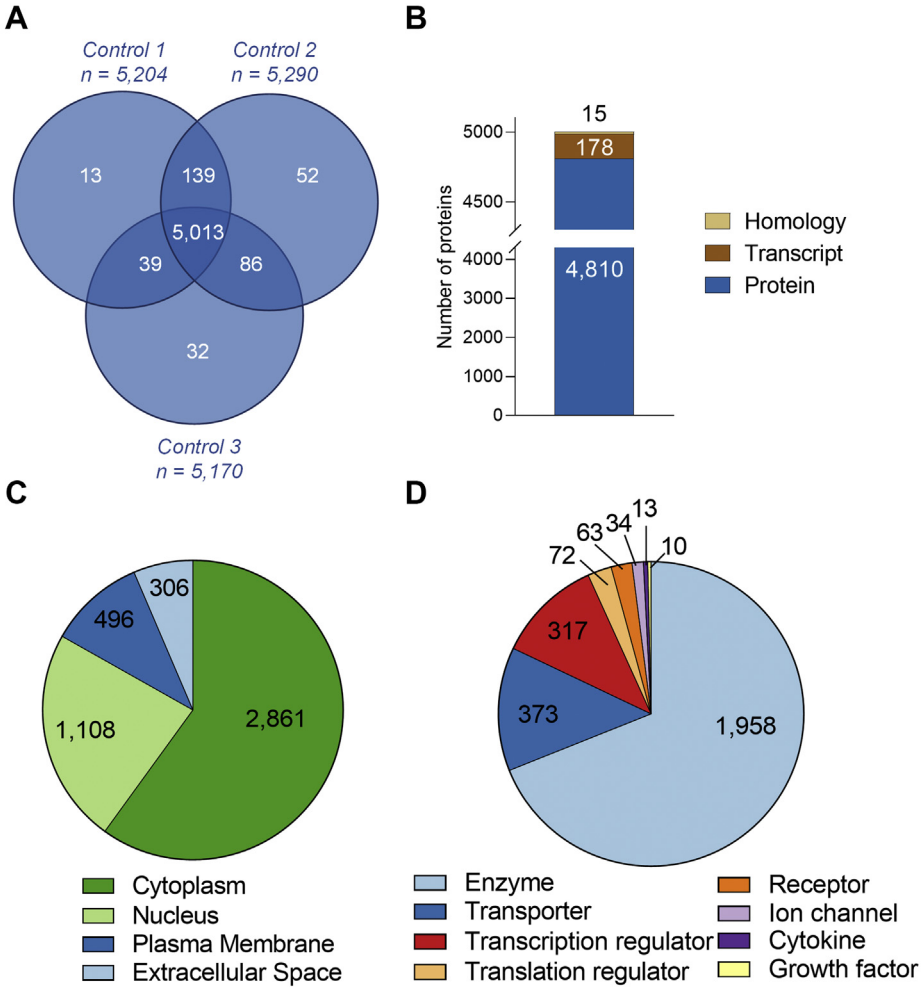

FIG. 2. **Characterization of the mouse seminal vesicle proteome.** *A*, proteins identified from each biological replicate of control treated mice were compared, with proteins identified in all three replicates constituting the core seminal vesicle proteome. *B*, using UniProt, the core proteome was then assessed to determine whether the proteins had annotated evidence at protein or transcript level or had been inferred from homology. An initial characterization of the core seminal vesicle proteome using Ingenuity Pathway Analysis revealed: (*C*) cellular localization and (*D*) protein classification.

associated with the seminal vesicle proteome (supplemental Table S4).

To identify the key regulators of the seminal vesicles, we then utilized the predictive upstream regulator function of Ingenuity Pathway Analysis. Among the curated regulators, those associated with cell proliferation and protein synthesis were highly predicted, including: RICTOR (p = 2.72E-53, 188 targets), transcriptional regulator tumor protein p53 (TP53) (p = 1.18E-52, 515 targets), MLX-interacting protein-like (MLXIPL, p =5.1E-30, 86 targets), and Myc proto-oncogene protein (MYC, p = 3.25E-21, 132 targets) (Fig. 3*B*, supplemental Table S5).

To provide a snapshot of the localization of proteins mapping to the proteome of seminal vesicles, a subset of proteins that were associated with seminal vesicle molecular functions identified in our *in silico* analysis were selected for validation by immunolocalization analysis (Fig. 3, *C–F*). Of these, RNA-binding protein Musashi homolog 2 (MSI2), which was associated with "cellular growth and proliferation" (p = 8.5E-10) and known to govern epithelial cell migration (50), was expressed in epithelial cells (predicted cytoplasm) (Fig. 3*C*). Additionally prosaposin (PSAP) (51), lysosomal acid lipase/cholesteryl ester hydrolase (LIPA) (52), and cluster of differentiation 9 antigen (CD9) (53), with revealed molecular and cellular functions related to cellular stress, "cell death and survival" (p = 6.5E-53), "cellular function and maintenance" (p = 2.6E-16), and "cellular compromise" (p = 2.5E-9), were investigated. Immunolocalization analysis revealed PSAP to be expressed in the smooth muscle layer (predicted extracellular space) (Fig. 3*D*), LIPA presents in the epithelium and smooth muscle layer (predicted cytoplasm) (Fig. 3*E*), and CD9

TABLE 1
Seminal vesicle proteome summary

	Number of proteins			
Group	n = 3 FDR ≤ 0.01	Av. peptide hits/protein	Av. unique peptide hits/protein	Av. protein coverage (%)
Control	5013	16.4	14.9	39.8
Acrylamide	4819	16.9	15.3	40.8

expression localized to the epithelium (predicted plasma membrane) (Fig. 3*F*).

Comparative Analysis of the Global Seminal Vesicle Proteome to Proteins Expressed in Seminal Vesicle Fluid

The primary function of the seminal vesicles is to synthesize and secrete a diversity of bioactive factors, including proteins that support gamete function and promote reproductive success (1, 2, 4). To compare our core proteome (supplemental Table S2) to proteins secreted in seminal vesicle fluid, we obtained seminal vesicle fluid proteomic data from Bayram *et al.*, 2020 (42), Chang *et al.*, 2010 (43), and Dean *et al.*, 2009 (44). Filtering this data for proteins reviewed by UniProt identified 58 proteins in common with one or more of the previous studies, including 26, 47, and 26 in common with the Bayram, Chang, and Dean studies respectively. Of these, all were detected in our core seminal vesicle proteome (Table 2, supplemental Table S2), and these included the well-characterized seminal vesicle secretory (SVS) protein family members: 3a, 4, 5, 6, prostate and testis-expressed 4 (PATE4), glia-derived nexin (SERPINE2), protein-glutamine gamma-glutamyltransferase 4 (TGM4), and serine protease inhibitor kazal-like protein, minor form (SPINKL), which have established physiological functions in copulatory plug formation and the modulation of sperm fertilizing ability (2). Strikingly among the 58 proteins, 18/58 (31%) were in the top 1% and 34/58 (59%) were in the top 10% of the most abundant proteins detected in the core seminal vesicle proteome (Table 2).

Acute Acrylamide Exposure Alters the Seminal Vesicle Proteome

We have previously demonstrated that paternal acrylamide exposure alters sperm quality in a manner that has consequences for fetal development (22). To examine whether acrylamide also dysregulates seminal vesicle function, male mice were subjected to an established acute acrylamide exposure protocol (22), whereby the animals received daily injections of either acrylamide or PBS (control) for five consecutive days prior to seminal vesicle tissue collection 72 h after the final injection (Fig. 1).

The treatment regimen did not substantially alter mouse body weight (Fig. 4*A*) or change seminal vesicle weight (Fig. 4*B*), but did elicit marked changes in the proteomic composition of the seminal vesicle tissue. A global analysis of the seminal vesicle tissue proteome from acrylamide-treated males returned high confidence identification of 4819 proteins (*FDR* ≤ 0.01, Fig. 4*C*, supplemental Table S6), with strong Pearson correlation coefficients (0.925 average r^2) across all biological replicates (supplemental Fig. S1*D*). Consistent with the depth of coverage achieved in control samples, an average of 16.9 peptides (15.3 unique peptides), representing a coverage of 40.8% per protein (Table 1), were identified per protein in the seminal vesicle tissue sourced from acrylamide-treated animals. Combined analysis of acrylamide (4819 proteins; Fig. 4*C*, supplemental Table S6) and control seminal vesicle proteomes (5013 proteins; Fig. 2*A*, supplemental Table S2) identified 5478 proteins (*FDR* ≤ 0.01). Filtering for proteins with three quantitative values in at least one treatment group (*i.e.*, control or acrylamide), and either 3 or 0 quantitative values in the opposing group, resulted in a final proteome of 4698 proteins (Fig. 4*D*, supplemental Table S7). Among these, three were exclusively identified in control seminal vesicle tissue: myelin protein P0 (MPZ), heterogeneous nuclear ribonucleoproteins C1/C2 (HNRNPC), and UDP-glucuronosyltransferase 1A7 (UGT1A7C). Five proteins were uniquely identified in acrylamide-exposed seminal vesicle tissue: WD repeat-containing protein 46 (WDR46), Rho GTPase-activating protein 10 (ARHGAP10), B-cell receptor-associated protein 29 (BCAP29), interleukin-1 receptor-associated kinase 4 (IRAK4), and DnaJ homolog subfamily B member 5 (DNAJB5) (Fig. 4, *D* and *E*). Additional analysis of the 4698 identified proteins using the Mouse Genome Informatics Phenotypes/Alleles project as well as the International Mouse Phenotyping Consortium databases revealed that 60/4698 (1.3%) proteins are associated with phenotypes in seminal vesicle structure or function (60 proteins) (supplemental Table S7).

Assessment of differentially regulated proteins in mouse seminal vesicles revealed a subset of proteins that were altered in response to acrylamide exposure. Initially, global assessment of protein profiles using principal component analysis demonstrated biological variance among the control mice but notably a tighter clustering among the acrylamide-treated mice, indicative of a consistent response to this reproductive toxicant (Fig. 5*A*). Assessment of the regulation of individual proteins demonstrated that 205 proteins were upregulated and 106 downregulated (fold-change ≥1.5 or ≤−1.5 and $p \leq 0.05$) (Fig. 5*B*, supplemental Table S7). These

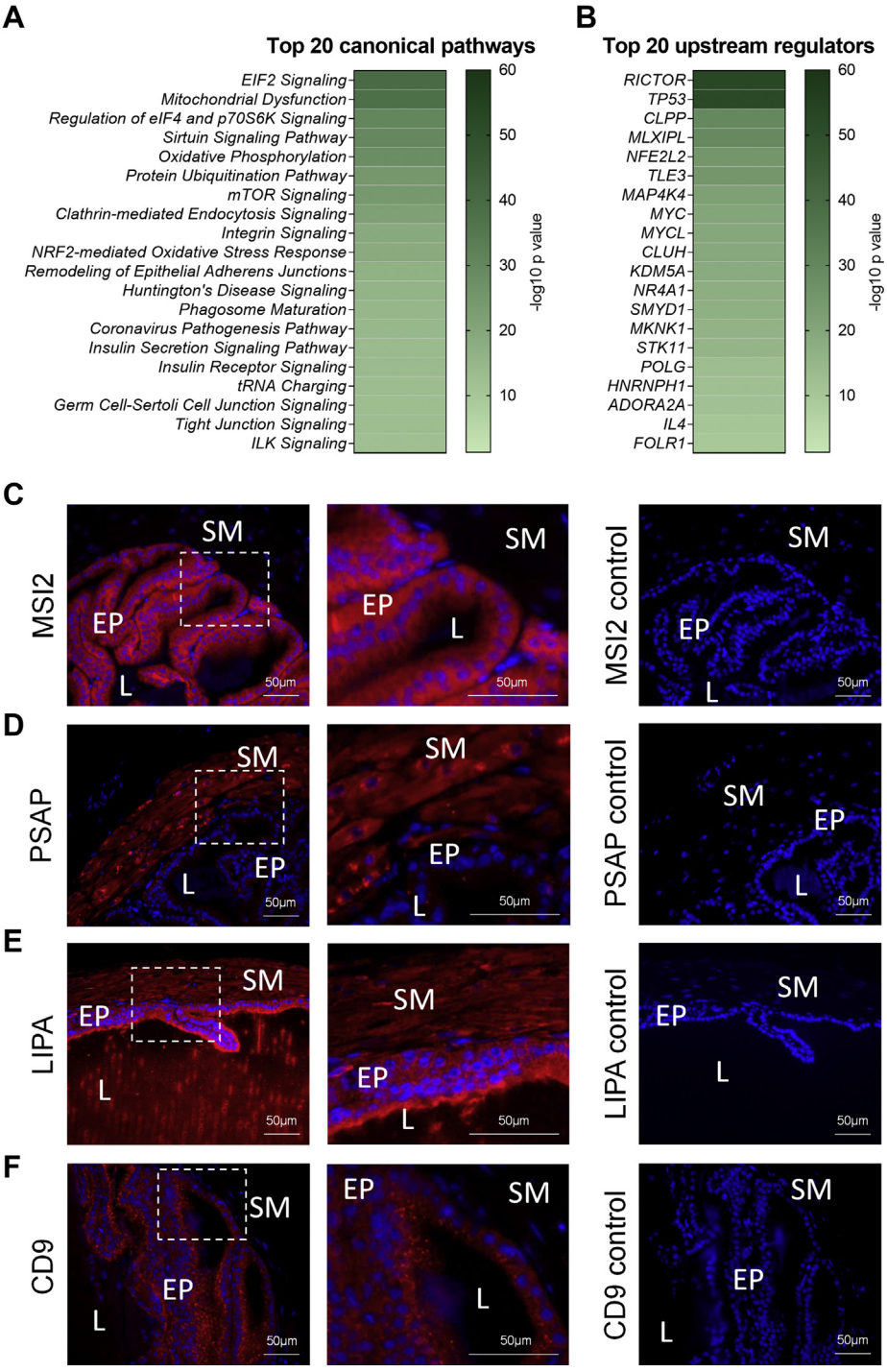

FIG. 3. **Functions of proteins expressed in the mouse seminal vesicle.** Functions of the mouse core seminal vesicle proteome were assessed by Ingenuity Pathway Analysis. This analysis was used to predict canonical signaling pathways and upstream regulators of the proteins expressed that were highly ($p \leq 0.05$) predicted to be involved in mouse seminal vesicle function. Data depicted represents the top 20: (*A*) canonical signaling pathways and (*B*) upstream regulators, presented as a heat map based on –log10 *p* values. A subset of proteins from the mouse seminal vesicle proteome were selected for immunofluorescence confirmation (n = 4). Candidate proteins were selected based on their association with functions of the seminal vesicle, including cellular proliferation/protein synthesis and cell death and survival. Representative images of low and high magnification and secondary antibody only controls for (*C*) RNA-binding protein Musashi homolog 2 (MSI2), (*D*) prosaposin (PSAP), (*E*) lysosomal acid lipase/cholesteryl ester hydrolase (LIPA), and (*F*) cluster of differentiation 9 antigen (CD9). *White boxes* indicate regions focused on for high power. EP, Epithelial cells; L, Seminal vesicle lumen; SM, Smooth muscle.

TABLE 2
Comparative analysis of the core seminal vesicle proteome to seminal vesicle fluid proteome

Accession	Description	Gene symbol	Coverage [%]	# Peptides	# Unique peptides	Order of abundance in core proteome
P18419	Seminal vesicle secretory protein 4	Svs4	80	20	20	1
P30933	Seminal vesicle secretory protein 5	Svs5	80	18	18	2
Q64356	Seminal vesicle secretory protein 6	Svs6	72	21	21	5
Q09098	Prostate and testis expressed protein 4	Pate4	64	13	13	6
Q61400	Carcinoembryonic antigen-related cell adhesion molecule 10	Ceacam10	79	23	22	7
Q8BZH1	Protein-glutamine gamma-glutamyltransferase 4	Tgm4	94	90	89	9
F2Z472	Seminal vesicle secretory protein 3A	Svs3a	84	37	37	10
P01887	Beta-2-microglobulin	B2m	70	11	11	11
P20029	Endoplasmic reticulum chaperone BiP	Hspa5	83	85	83	12
P09036	Serine protease inhibitor Kazal-type 1	Spink3; Spink1	64	13	13	15
P09103	Protein disulfide-isomerase	P4hb	91	76	76	18
P10126	Elongation factor 1-alpha 1	Eef1a1	81	51	33	19
P07724	Serum albumin	Alb	93	91	91	21
P45376	Aldo-keto reductase family 1 member B1	Akr1b3	74	35	34	26
P14211	Calreticulin	Calr	78	44	44	30
Q07235	Glia-derived nexin	Serpine2	74	33	33	33
Q8BND5	Sulfhydryl oxidase 1	Qsox1	70	59	7	36
P81117	Nucleobindin-2	Nucb2	85	69	69	46
Q921I1	Serotransferrin	Trf	72	70	70	52
P35700	Peroxiredoxin-1	Prdx1	95	32	30	62
P17182	Alpha-enolase	Eno1	91	50	43	74
Q01853	Transitional endoplasmic reticulum ATPase	Vcp	86	107	106	75
P24369	Peptidyl-prolyl *cis-trans* isomerase B	Ppib	75	30	30	76
Q8CEK3	Serine protease inhibitor kazal-like protein, minor form	Spinkl	52	9	9	92
P21460	Cystatin-C	Cst3	66	14	14	105
P18242	Cathepsin D	Ctsd	64	27	27	112
P06869	Urokinase-type plasminogen activator	Plau	78	36	36	124
P13020	Gelsolin	Gsn	68	49	49	164
P07759	Serine protease inhibitor A3K	Serpina3k	54	29	27	251
O09159	Lysosomal alpha-mannosidase	Man2b1	51	47	47	252
Q9QY48	Deoxyribonuclease-2-beta	Dnase2b	43	20	20	259
P22599	Alpha-1-antitrypsin 1–2	Serpina1b	65	31	12	285
Q3UN54	Secreted seminal-vesicle Ly-6 protein 1	A630095E13Rik	54	6	6	325
P12032	Metalloproteinase inhibitor 1	Timp1	59	12	12	431
Q61207	Prosaposin	Psap	57	24	24	509
P28665	Murinoglobulin-1	Mug1	54	59	37	519
P28798	Progranulin	Grn	71	32	32	523
P32261	Antithrombin-III	Serpinc1	69	33	33	583
P01027	Complement C3	C3	69	103	103	669
O88968	Transcobalamin-2	Tcn2	79	22	22	808
Q9Z0J0	NPC intracellular cholesterol transporter 2	Npc2	59	17	17	846
P06728	Apolipoprotein A-IV	Apoa4	74	27	27	923
Q06890	Clusterin	Clu	33	17	17	953
E9Q557	Desmoplakin	Dsp	38	86	86	995
Q9D309	Protein FAM3B	Fam3b	70	19	19	1028
P11276	Fibronectin	Fn1	40	61	61	1073
P21614	Vitamin D-binding protein	Gc	81	33	33	1092
P23953	Carboxylesterase 1C	Ces1c	35	17	14	1324
P06797	Cathepsin L1	Ctsl	56	16	16	1363
Q01339	Beta-2-glycoprotein 1	Apoh	48	17	17	1628
P20918	Plasminogen	Plg	51	31	31	1864
Q62181	Semaphorin-3C	Sema3c	39	20	20	1936
P11672	Neutrophil gelatinase-associated lipocalin	Lcn2	44	6	6	1982
Q9QZL9	Dickkopf-like protein 1	Dkkl1	40	10	10	2154

TABLE 2—*Continued*

Accession	Description	Gene symbol	Coverage [%]	# Peptides	# Unique peptides	Order of abundance in core proteome
P13634	Carbonic anhydrase 1	Car1	58	11	11	2239
P07309	Transthyretin	Ttr	71	8	8	2259
Q9ESB3	Histidine-rich glycoprotein	Hrg	25	12	12	2997
Q00897	Alpha-1-antitrypsin 1–4	Serpina1d	48	23	2	3714

The core seminal vesicle fluid proteome was determined as described in supplemental Table S2 and compared with a high confidence mouse seminal vesicle fluid proteome. This high confidence proteome was generated by obtaining data from Bayram *et al.*, 2020 (42), Chang *et al.*, 2010 (43), and Dean *et al.*, 2009 (44) and filtering this data to only include proteins reviewed by UniProt. This led to a final high confidence list of 58 proteins. Included in this dataset is the order of abundance in the core proteome, determined by the average of normalized abundance quants of the three biological replicates (prior to scaling), to demonstrate the relative level of expression of seminal vesicle secreted proteins within the proteome.

significantly regulated proteins ranged in abundances (supplemental Fig. S1*E*) and 8/311 (2.6%) were associated with seminal vesicle phenotypes (Table 3).

Functional assessment of the differentially expressed proteins using Ingenuity Pathway Analysis (Fig. 6, supplemental Fig. S2, supplemental Tables S8–S10) revealed that canonical pathways and molecular functions dysregulated following acrylamide exposure were associated with the regulation of protein synthesis and cellular stress (Fig. 6, *A* and *C*, supplemental Fig. S2, *A–C* and supplemental Tables S8 and

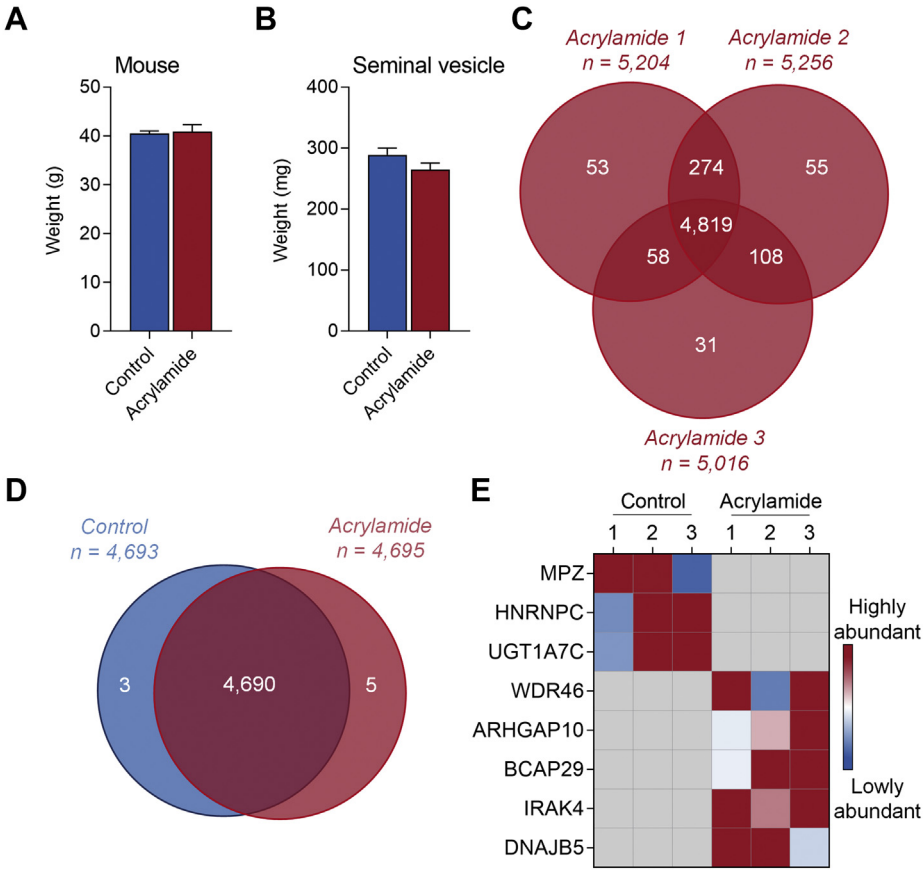

FIG. 4. **Characterization of the mouse seminal vesicle proteome following acrylamide exposure.** *A*, mouse weight (g) (n = 7 individual mice per treatment group) and (*B*) seminal vesicle weight (mg) (n = 11 individual mice per treatment group) were initially assessed prior to isolation of proteins. Data are presented as a column graph with mean ± SEM values and analyzed by unpaired *t* test with significance indicated (*) if $p \leq 0.05$ when comparing the acrylamide to the control group. Using a Venn diagram, (*C*) proteins detected across the n = 3 replicates of the acrylamide group were determined, (*D*) then compared with the control group filtering for proteins with three quantitative values in at least one of control or acrylamide groups, and either 3 or 0 quantitative values in the other group. *E*, proteins identified as unique to control or acrylamide are presented as a heat map.

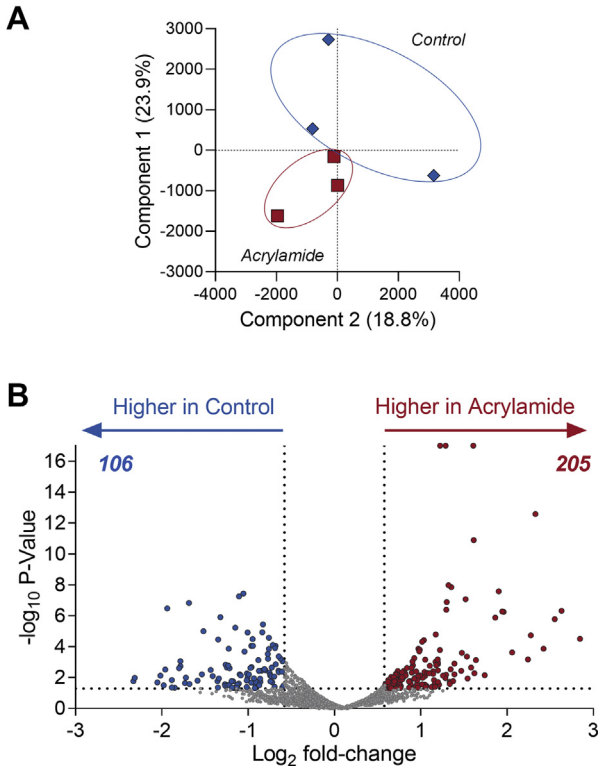

FIG. 5. **Acrylamide exposure alters the mouse seminal vesicle proteome.** Seminal vesicle proteomic data from acrylamide and control mice was assessed (n = 3 biological replicates per group) to identify those proteins with a fold-change ≥ 1.5 or ≤ −1.5 and $p \leq 0.05$ using Proteome Discoverer 2.4. *A*, principal component analysis of proteomic data. *B*, graphical depiction of differentially regulated proteins using a volcano plot.

S9). Utilization of a Z-score algorithm to assign either pathway activation (Z-score ≥ 2) or inhibition (Z-score ≤ −2) revealed EIF2 signaling (Z-score = 3.46), which is associated with eukaryotic protein synthesis (54), as predicted to be activated in acrylamide-exposed seminal vesicles, while death receptor signaling (Z-score = −2), associated with cellular stress and apoptosis (55), was predicted to be inhibited (Fig. 6*C*). Interestingly, assessment of molecular and physiological functions revealed a large number of proteins associated with the terms "cell death and survival" and "cell proliferation/protein synthesis" (supplemental Fig. S2*A*), with overrepresentation of the functions "apoptosis" in the category "cell death and survival" and "translation of protein" in the category "protein synthesis" (supplemental Fig. S2, *B* and *C*, supplemental Table S9).

To identify the upstream signaling pathways involved in transmitting the acrylamide-mediated dysregulation of mouse seminal vesicle function, we utilized the upstream regulator function of Ingenuity Pathway Analysis. A total of 206 upstream factors were predicted to be regulators of the seminal vesicle response to acute acrylamide exposure ($p \leq 0.05$, supplemental Table S10). To assess the activation or inhibition status of these regulators, we first filtered to remove all chemical molecules other than those classified as endogenous mammalian chemicals, leaving 156 predicted upstream regulators ($p \leq 0.05$, Fig. 6*B*, supplemental Table S10). Of these, four were predicted to be activated (Fig. 6*D*) including MLXIPL, MYC, N-myc proto-oncogene protein (MYCN), and Rho family of GTPases (RHO), while the four inhibited regulators included RICTOR, La-related protein 1 (LARP1), cyclin-dependent kinase 4/6 (CDK4/6), and miRNA-210 (Fig. 6*D*, supplemental Fig. S2, *D–F*, supplemental Table S10).

Notably RICTOR, a major component of the mTOR signaling pathway known to influence both protein synthesis (56) and epithelial cell function (57, 58), was a predicted upstream regulator identified in the core mouse seminal vesicle proteome (p = 2.52E-53, Fig. 3*B* and supplemental Table S5) and was also prominent among dysregulated upstream regulators

TABLE 3
Comparative analysis of the seminal vesicle proteome to seminal vesicle phenotypes identified from the Mouse Genome Informatics and The International Mouse Phenotyping Consortium datasets

Accession	Protein names	Gene symbol	FC (acrylamide *versus* control)	*p*-value	Phenotype description
Q61103	Zinc finger protein ubi-d4	Dpf2	2.14	5.10E-03	abnormal seminal vesicle morphology
Q9D1Q4	Dolichol-phosphate mannosyltransferase subunit 3	Dpm3	1.83	1.66E-02	abnormal seminal vesicle morphology
Q9D142	Uridine diphosphate glucose pyrophosphatase NUDT14	Nudt14	1.62	1.71E-02	abnormal seminal vesicle morphology
P63037	DnaJ homolog subfamily A member 1	Dnaja1	1.58	8.86E-03	small seminal vesicle
Q61792	LIM and SH3 domain protein 1	Lasp1	1.57	1.32E-02	small seminal vesicle
Q8C5P7	Testis development-related protein	Tdrp	−1.52	4.10E-03	abnormal seminal vesicle morphology
P06869	Urokinase-type plasminogen activator	Plau	−1.56	4.37E-04	herniated seminal vesicle
Q9Z0M9	Interleukin-18-binding protein	Il18 bp	−2.35	1.66E-03	abnormal seminal vesicle morphology

Seminal vesicle phenotypes associated with proteins expressed in the mouse seminal vesicle were determined. These data were then filtered based upon those proteins that met our differential regulation criteria (−1.5 ≤ FC ≥ 1.5, $p \leq 0.05$) and proteins that matched these criteria are presented along with their associated phenotypes.

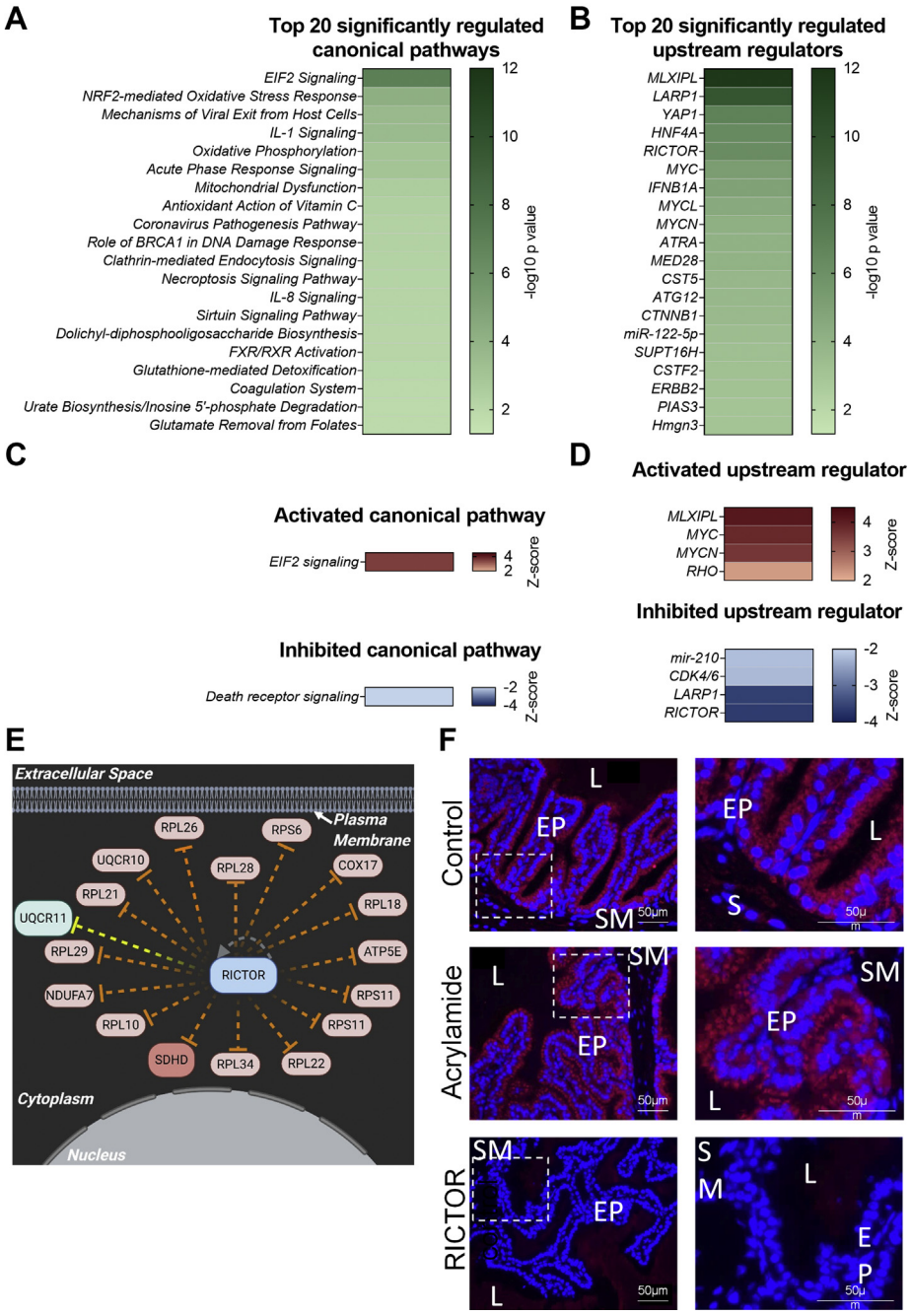

FIG. 6. **Signaling pathways and upstream regulators influenced by acrylamide exposure in the mouse seminal vesicles.** Ingenuity Pathway Analysis was used to predict ($p \leq 0.05$) canonical signaling pathways and upstream regulators of the mouse seminal vesicle proteins that were differentially regulated following acrylamide treatment. Data are represented as a heat map based on –log10 p values and show the top 20: (*A*) canonical signaling pathways and (*B*) upstream regulators. To gain a greater understanding of the regulation of these pathways, (*C*) canonical signaling pathways and (*D*) upstream regulators that were predicted to be activated (Z-score ≥ 2) or inhibited (Z-score ≤ –2) with $p \leq 0.05$ are represented as heat maps based on Z-score value. *E*, proteins differentially expressed following acrylamide exposure (*red* = upregulated, *green* = downregulated) that are documented to be regulated by RICTOR are presented in an interaction network. *Connecting lines* indicate several predicted relationships that lead to activation (*orange*) and a relationship not consistent with that published in the literature (*yellow*). Image created with BioRender.com. *F*, representative images from immunofluorescence analysis of RICTOR in control and acrylamide samples at low and high power and secondary antibody only controls (n = 5/group). *White boxes* indicate regions focused on for high power. EP, Epithelial cells; L, Seminal vesicle lumen; SM, Smooth muscle.

following acrylamide exposure (Z-score = –3.64, p = 6.69E-07. Fig. 6, *B*, *D–F* and supplemental Table S10), despite not having altered expression (1.2 fold-change, p = 6.4E-01, supplemental Table S7). As a prelude for future studies focusing on defining the regulatory role of RICTOR in seminal vesicle tissues, we used immunofluorescence to assess the distribution of the protein in both control and acrylamide-treated tissue samples. This approach revealed intense RICTOR labeling that was primarily associated with the apical surface of seminal vesicle epithelial cells, yet failed to respond in terms of either abundance or localization upon acrylamide challenge (Fig. 6*F*).

To validate differential protein expression, a subset of proteins whose expression was dysregulated by acrylamide treatment and that were associated with responsive cellular and molecular functions identified by bioinformatic analyses were selected for orthogonal quantification by immunoblotting (n = 4 per group). Specifically, these proteins were associated with "cell death and survival"; Caspase-6 (CASP6, –1.71-fold-change in acrylamide *versus* control, p = 2.91E-04), or "protein synthesis"; (60S ribosomal protein L28 (RPL28, 1.96-fold-change in acrylamide *versus* control, p = 1.33E-04), and eukaryotic translation initiation factor 4E-binding protein 1 (EIF4EBP1, –2.06-fold-change in acrylamide *versus* control, p = 2.06E-04)). Additionally, we also assessed Lactadherin (MFGE8, –1.2-fold-change in acrylamide *versus* control, p = 6.83E-01) as a protein that did not exhibit change in the proteomic dataset. Consistent with the proteomic data, CASP6 (Fig. 7, *A* and *B*, –1.9-fold-change in acrylamide *versus* control, p = 0.0021), and EIF4EBP1 (Fig. 7, *A* and *C*, –1.8-fold-change in acrylamide *versus* control, $p < 0.0001$) were suppressed, while RPL28 (Fig. 7, *A* and *D*, 1.8 fold-change in acrylamide *versus* control, p = 0.0005) was induced following acrylamide exposure. Additionally, MFGE8 (Fig. 7, *A* and *E*, 1.23 fold-change in acrylamide *versus* control, p = 0.1420) was not altered.

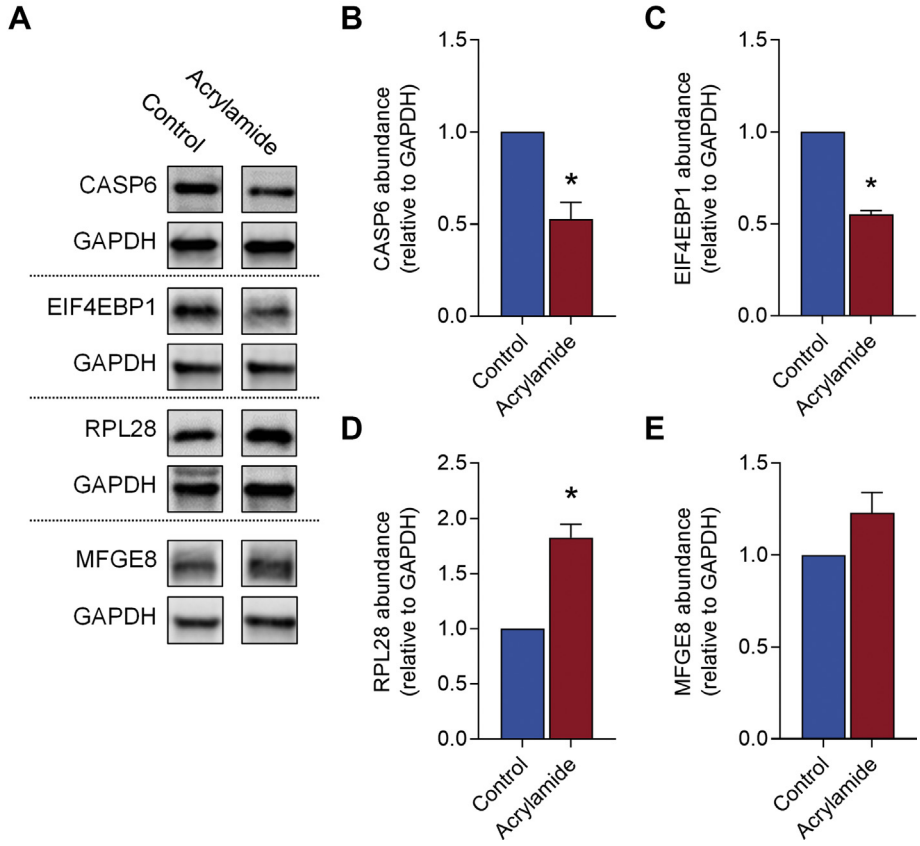

FIG. 7. **Orthogonal validation of proteins identified in the mouse seminal vesicle proteome.** Quantitative mass spectrometry data were validated *via* immunoblotting of differentially regulated proteins (n = 4 individual mice per treatment group). Candidate proteins were selected based on those differentially regulated proteins that were associated with canonical pathways and upstream regulators with (*A*) Representative Immunoblotting images shown. Proteins assessed included (*A* and *B*) Caspase-6 (CASP6), (*A* and *C*) Eukaryotic translation initiation factor 4E-binding protein 1 (EIF4EBP1), (*A* and *D*) 60S ribosomal protein L28 (RPL28), and (*A* and *E*) lactadherin (MFGE8). Immunoblotting data were assessed using Multi Gauge software, normalized to the control group and presented as a column graph with mean ± SEM values. Data were analyzed by unpaired *t* test. * $p \leq 0.05$ indicates statistical significance when comparing acrylamide with control groups.

Acrylamide Treatment Leads to Increased Levels of Oxidative DNA Damage in the Mouse Seminal Vesicle

We have previously demonstrated that exposure to acrylamide leads to increased levels of oxidative DNA damage in epididymal sperm (22–24, 59). Consistent with these findings, we observed a number of canonical signaling pathways and functions associated with the cellular response to oxidative stress that were altered in the mouse seminal vesicles following acrylamide exposure (Fig. 6, supplemental Tables S8 and S9). These pathways included NRF2-mediated oxidative stress response (11 proteins, p = 6.92E-05), acute-phase response signaling (9 proteins, p = 9.12E-04), antioxidant actions of vitamin C (6 proteins, p = 4.17E-03), sirtuin signaling pathway (10 proteins, p = 7.59E-03), glutathione-mediated detoxification (3 proteins, p = 9.77E-03) (Fig. 6*A* and supplemental Table S8), and free radical scavenging (22 proteins, p = 3.69E-03) (Fig. 8*A* and supplemental Table S9). Given this evidence, we assessed whether acrylamide exposure causes oxidative stress in seminal vesicle tissues. Specifically, seminal vesicle tissue sections were assessed for their levels of oxidative DNA damage burden using an 8-OHdG probe. This analysis confirmed that acrylamide treatment elicits elevated 8-OHdG in epithelial cells (Fig. 8, *B* and *D*, fivefold increase, p = 0.016) and the smooth muscle cell layer (Fig. 8, *C* and *D*, twofold increase, p = 0.04).

Acrylamide Treatment Leads to Alterations of Seminal Vesicle Secretory Capacity

Collectively, these data demonstrate that seminal vesicle tissue is responsive to acute acrylamide exposure; however, whether these changes alter the secretory capacity of the seminal vesicles remained to be answered. To begin to address this question, we undertook histological analysis of seminal vesicles to examine the impact of acrylamide on epithelial cells and the smooth muscle layer, which play important roles in modulating secretory capacity (25). Analysis of seminal vesicle epithelial cells revealed no significant change in epithelial cell mucosal folding/branching (Fig. 9, *A* and *D*), nor any change in epithelial cell height, reflective of maintenance of a tall secretory columnar epithelium following acrylamide exposure (Fig. 9, *B* and *D*). Similarly, no significant change was observed in the depth of the smooth muscle cell layer (Fig. 9, *C* and *E*) in acrylamide-treated seminal vesicle tissue compared with the controls, suggesting that SVS capacity was unchanged.

However, despite not overtly affecting gross seminal vesicle morphology or weight (Fig. 4*B*, Fig. 9, *A*–*E*), acrylamide treatment did significantly reduce the volume of seminal vesicle secretions harvested from treated animals (Fig. 10*A*, 36% reduction, $p < 0.01$). Notably, this response was also reflected in a reduction in the total amount of seminal vesicle fluid protein collected (Fig. 10*B*, 25% reduction, p = 0.02), with a small but nonsignificant increase in protein concentration per mg fluid collected observed (Fig. 10*C*, p = 0.055).

Additionally, analysis of our proteomic data for seminal vesicle secreted proteins showed evidence of alterations to seminal vesicle secreted proteins (Table 2) (42–44). Seven of these, alpha-1-antitrypsin 1–4 (SERPINA1D, 5.0 FC, p = 2.56E-13), serine protease inhibitor A3K (SERPINA3K, 1.66 FC, p = 9.39E-03), carbonic anhydrase 2 (CAR1, 1.5 FC, p = 1.60E-2), urokinase-type plasminogen activator (PLAU, −1.56 FC, p = 4.4E-04), NPC intracellular cholesterol transporter 2 (NPC2, −1.6 FC, p = 8.0E-05), dickkopf-like protein 1 (DKKL1, −1.7 FC, p = 3.21E-03), and neutrophil gelatinase-associated lipocalin (LCN2, −1.9 FC, p = 9.0E-05) were significantly altered (FC $\geq$ 1.5 or $\leq$ −1.5 and $p \leq 0.05$) in seminal vesicle tissue of acrylamide-treated males compared with control (Fig. 10*D*, Table 2). Notably, of the 12 other seminal vesicle secreted proteins (supplemental Fig. S3, Table 2) that did not reach the effect size threshold but did reach statistical significance, seven were in the top 1% most abundant seminal vesicle proteins. These included PATE4 (−1.25 FC, p = 3.54E-02), SVS3A (−1.30 FC, p = 1.98E-02), carcinoembryonic antigen-related cell adhesion molecule 10 (CEACAM10, −1.34FC, p = 1.07E-02), serine protease inhibitor kazal-type 1 (SPINK1, −1.36 FC, p = 8.3E-03), beta-2-microglobulin (B2M, −1.37 FC, p = 7.28E-03) SVS6 (−1.41 FC, p = 4.34E-03), and sulfhydryl oxidase 1 (QSOX1, −1.44 FC, p = 2.73E-03) (supplemental Fig. S3, Table 2).

DISCUSSION

Supporting the delivery of spermatozoa to the site of fertilization has long been considered the sole function of seminal plasma, but this narrow delineation is now inadequate. Indeed, seminal plasma fulfills a more complex role in virtually all species that deposit gametes in the female reproductive tract at intromission (1). Thus, in addition to its primary function in sperm delivery, seminal plasma modifies the postcopulatory female reproductive tract environment in a manner that supports embryo implantation and exerts long-term consequences for offspring health (2, 3, 15, 21). In most species, the major contributor to seminal plasma volume is the seminal vesicle glands (2, 4). Although compelling evidence implicates these glands as crucial regulators of reproductive success (3, 15, 17), understanding of their physiology and proteomic constitution remains limited. This is illustrated through analysis of reviewed *M. musculus* proteins in UniProt (25,260 proteins) whereby only 26 proteins have been characterized as seminal vesicle expressed, despite substantially more proteins linked with seminal vesicle phenotypes (40, 41). Thus, in completing the first proteomic assessment of the mouse seminal vesicle, we have built greater understanding of this gland's complex biology and demonstrated that the seminal vesicle tissue, akin to that of other segments of the male reproductive tract, is sensitive to environmental exposures.

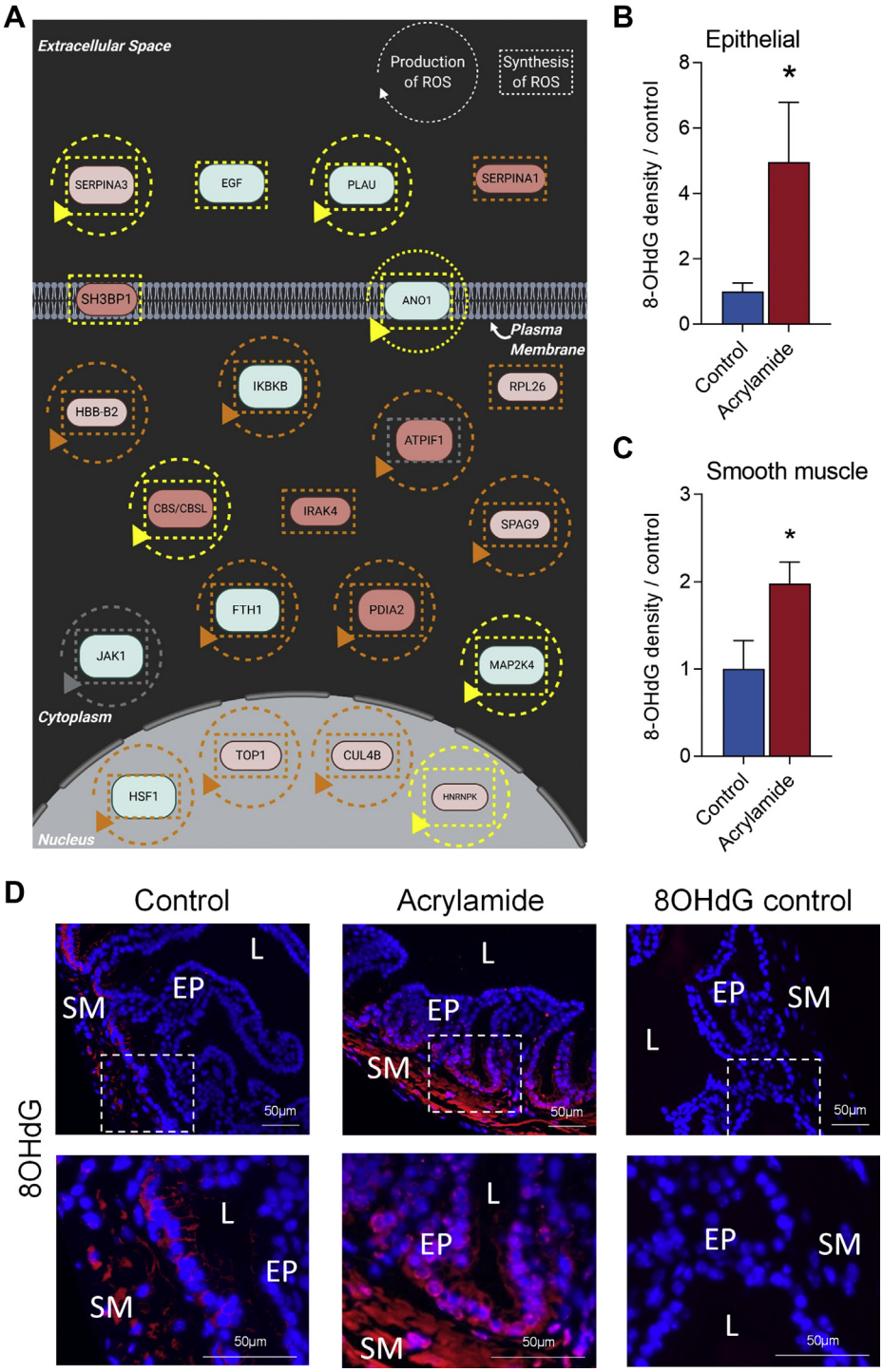

FIG. 8. **Acrylamide induces oxidative stress in the mouse seminal vesicle.** *A*, Ingenuity Pathway Analysis identified the production and synthesis of reactive oxygen species as a significant ($p \leq 0.05$) cellular function associated with proteins that were differentially regulated following acrylamide exposure. These data are presented as interaction networks where a *circular arrow* surrounding the protein name indicates it is associated with the production of reactive oxygen species, and a *square dotted line* surrounding the protein indicates it is associated with the synthesis of reactive oxygen species. These *lines* indicate several predicted relationships that lead to activation (*orange*), relationship inconsistent with the literature (*yellow*), and relationship is known but effects on function is yet to be completely characterized (*gray*). Image created with BioRender.com. *B–D*, oxidative DNA damage was measured using 8-Hydroxy-2' -deoxyguanosine (8-OHdG) in (*B*) epithelial cells and (*C*) the smooth muscle layer, with (*D*) representative images at low and high magnification and secondary antibody only controls (n = 5/group). *White boxes* indicate regions focused on for high power. Data were analyzed by unpaired *t* test and are presented as a column graph with mean ± SEM values. *$p \leq 0.05$ indicates statistical significance when comparing acrylamide with control groups. EP, Epithelial cells; L, Seminal vesicle lumen; SM, Smooth muscle.

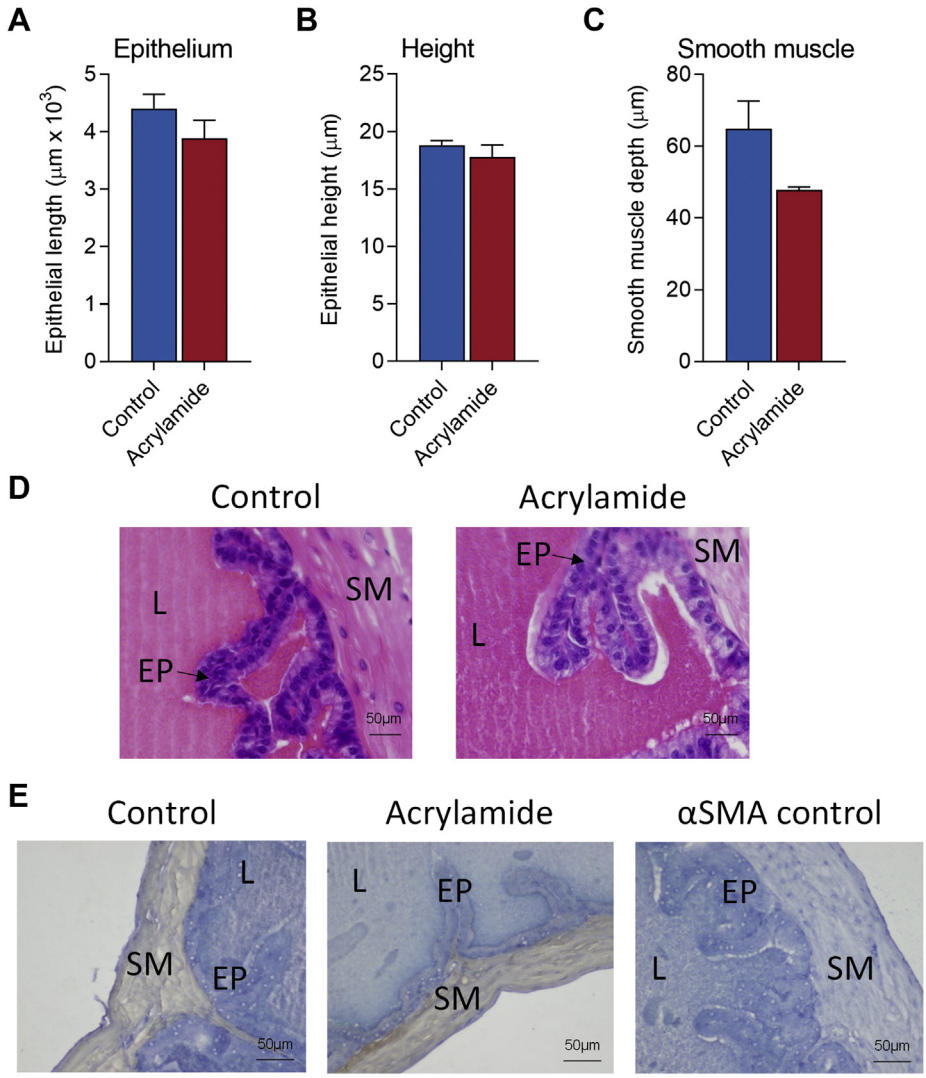

FIG. 9. **Seminal vesicle cellular structure is not altered following acrylamide exposure.** *A* and *D*, epithelial cell branching/folding (*B* and *D*) epithelial cell height, and (*C* and *E*) depth of stromal muscle layer wete assessed as surrogate measures of seminal vesicle secretory capacity with (*D* and *E*) representative histological images of (*D*) hematoxylin and eosin and (*E*) alpha smooth muscle actin (αSMA) presented. Data were analyzed by unpaired *t* test and are presented as column graphs with mean ± SEM values from n = 5 individual mice per group. EP, Epithelial cells; L, Seminal vesicle lumen; SM, Smooth muscle.

The principal responsibility of the seminal vesicles is to synthesize and secrete a diversity of bioactive factors, including proteins that promote reproductive success by supporting gamete function or interacting with the female reproductive tract (2, 4, 5). Consistent with this primary function, proteins secreted by the seminal vesicle (42–44) were among the most abundant proteins detected in seminal vesicle tissue. These proteins play critical roles in semen coagulation (*e.g.*, members of the SVS family and PATE4), and the regulation of male gamete function (*e.g.*, members of the SVS family, SPINKL and SERPINE2) (1–4). Consistent with other secretory mucosal surfaces, wherein equivalent cellular pathways mediate the cell fate decisions needed to maintain healthy tissue homeostasis and organ functionality (60–62), our *in silico* analysis of the seminal vesicle proteome identified cell proliferation, protein synthesis, and protein turnover as prominent biological processes. In addition, proteins linked to cellular death and survival pathways were abundantly represented within the seminal vesicle proteome.

Notably, the composition of seminal vesicle secretions is known to exhibit significant plasticity in response to changing paternal environments (63–65) or even cues produced by a female partner (66); functions that are postulated to maximize fertilization success and transmit evolutionary adaptations to offspring (63, 66, 67). These above studies raise the possibility that in addition to sperm, the seminal vesicles are sensitive to environmental signals and stressors (3, 15, 17). To assess the

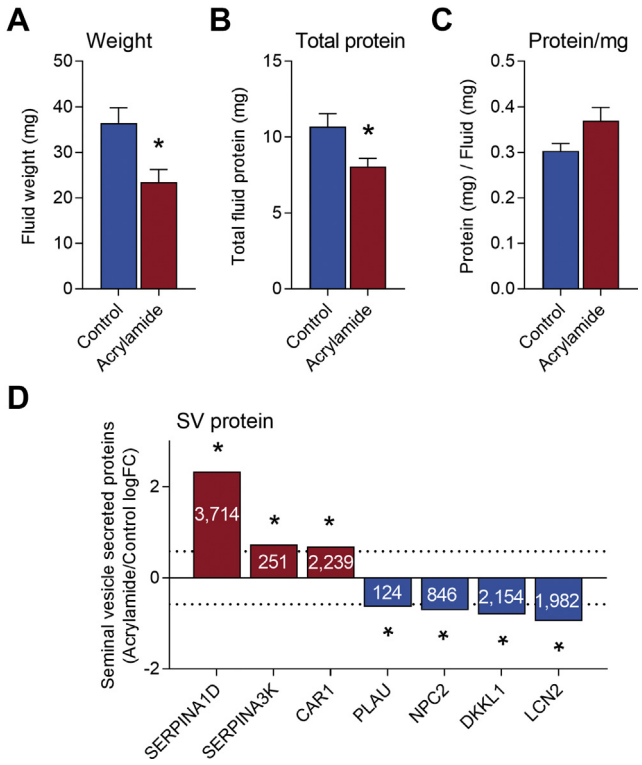

FIG. 10. **Seminal vesicle secretory function is perturbed following acrylamide exposure.** Seminal vesicle fluid was collected and (*A*) seminal vesicle fluid weight (mg), (*B*) total seminal vesicle fluid protein (mg), and (*C*) seminal vesicle fluid protein/mg seminal vesicle fluid were assessed. Data are presented as column graph with mean ± SEM values and data from n = 11 individual mice per treatment group. Data were analyzed by unpaired *t* test. *$p \leq 0.05$ indicates statistical significance. *D*, expression of seminal vesicle secreted proteins (n = 3 individual mice per treatment group) identified by proteomics of mouse seminal vesicle fluid (42–44) as statistically significant ($p \leq 0.05$ indicated by *) and fold-change ≥ 1.5 or ≤ −1.5 in our proteomic analysis. Proteins assessed included alpha-1-antitrypsin 1–4 (SERPINA1D), serine protease inhibitor a3k (SERPINA3K), carbonic anhydrase 2 (CAR1), urokinase-type plasminogen activator (PLAU), NPC intracellular cholesterol transporter 2 (NPC2), dickkopf-like protein 1 (DKKL1), and neutrophil gelatinase-associated lipocalin (LCN2). Data are presented as column graphs of log fold-change (logFC).

impact of environmental exposures on seminal vesicle function, we utilized a readily tractable *in vivo* acute acrylamide exposure model. This model, which utilizes doses of acrylamide that are substantially higher than human chronic exposure estimates (68), has been extensively utilized by us (22) and others (69, 70) to investigate adverse impacts of acrylamide exposure on sperm quality and fetal development. Specifically, exposure of testicular germ cells to acrylamide leads to enhanced levels of DNA damage that fail to be resolved during sperm maturation, yet do not appear to affect fetal development. Comparable levels of DNA damage are also characteristic of sperm exclusively exposed to acrylamide during epididymal transit. However, exposure during epididymal transit leads to substantially increased rates of fetal loss (22, 69, 71, 72). This raises the intriguing possibility that the male transfers the burden of acrylamide stress to the female through mechanisms that are independent of sperm DNA damage. While the nature of these paternal stress signals and the timing of their transfer to spermatozoa remain an area of active investigation, our data raise the prospect that other tissues in the male reproductive tract such as the seminal vesicles may be similarly affected by paternal stressors and therefore deserve consideration in terms of a holistic appraisal of their impact on male reproductive health and fertility.

Consistent with this possibility, paternal exposure to the reproductive toxicant, acrylamide altered the seminal vesicle proteome. *In silico* analysis of the dysregulated proteins provided evidence that the seminal vesicles initiate protein synthesis and promote cellular survival in response to the acrylamide insult, in order to return seminal vesicle tissue to normal homeostasis and functionality. The cellular responses we observed among dysregulated proteins share analogy with changes recorded following oxidative stress insults, wherein cells typically increase the expression of antioxidant genes and activate pathways that promote survival and adaptation to counter the cytotoxic effects of excessive reactive oxygen species production (73). Indeed, our studies demonstrate that treatment with the antioxidant resveratrol for 3 months rescues acrylamide-induced sperm DNA damage in mouse chronic exposure model (59), but this rescue is lost after a longer, 6 month exposure when other consequences of treatment have become apparent. Similarly, other studies have demonstrated that antioxidants can inhibit oxidative stress in rodent seminal vesicles (74, 75). Here we demonstrate that acrylamide exposure leads to the dysregulation of oxidative stress pathways accompanied by elevation of 8-OHdG lesions in the seminal vesicle epithelium, indicating that oxidative stress likely plays a leading role in the pathological response of this tissue to acute acrylamide.

Notably in our analysis, we have detected proteins uniquely expressed in the seminal vesicle proteome, with ARHGAP10, BCAP29, DNAJB5, IRAK4, and WDR46 present following acrylamide treatment and HNRNPC, MPZ, and UGT1A7C absent. In agreement with our *in silico* analysis, these uniquely acrylamide-expressed proteins are associated with driving cellular maintenance, proliferation, and repair in response to cellular stressors. Specifically, DNAJB5, a member of the heat shock protein 40 chaperone family (76), is a regulator of cellular protein homeostasis through its interaction with histone deacetylases and is activated in response to oxidative stress (77, 78). Moreover, the expression of DNAJB5 is known to increase in response to other cellular stressors such cancer (79) or infection (80).

Notwithstanding the paucity of studies focused on changes to the global proteomic landscape induced by acrylamide challenge in other tissues, we sought to explore the conservation of the proteomic response of the seminal vesicles to

that of other tissues. We noted a 68% overlap (23/34) between proteins identified within our dataset and significantly dysregulated proteins identified in hippocampal tissue (81) and striatal synaptosomes (82) (supplemental Table S11). However, of the 23 detected proteins, only glutathione S-transferase omega-1 (upregulated) and alpha-soluble NSF attachment protein (downregulated) were also significantly dysregulated in seminal vesicle tissue. Although these studies suggest that the seminal vesicles respond to acrylamide in a tissue-specific manner compared with existing data (81, 82), further studies are required to confirm this, particularly through the examination of proteomic changes in response to acrylamide from other male reproductive tract tissues.

Much of our knowledge of seminal vesicle biology comes from studies examining the impact of androgens on this tissue. Indeed, androgens are pivotal for all aspects of seminal vesicle development and function through their capacity to trigger differentiation of epithelial cells into a secretory epithelial layer (4, 25, 83). This raises the possibility that dysregulated production of androgens may contribute to altered seminal vesicle function following acrylamide exposure. However, we did not observe the expected reduction in seminal vesicle size or tissue morphology (84), nor did we detect any *in silico* evidence of endocrine pathway disruption. These findings suggest that our subchronic acrylamide exposure regimen was below the threshold needed to influence serum testosterone levels (85, 86), and thus androgens are unlikely to be solely responsible for driving the seminal vesicle response to acrylamide.

Due to the lack of comprehensive assessment of the proteomic composition of seminal vesicles, the identity of other regulators of seminal vesicle function remains unknown, although estrogens (87) and sexual activity (88) are implicated. In an attempt to shed light on novel regulators, we utilized Ingenuity Pathway Analysis to identify regulators of central importance to the seminal vesicle. Notably, *in silico* analyses identified RICTOR, a component of the mTOR pathway with established roles in protein production, protein secretion, and epithelial cell function (56–58, 89–94), as a putative regulator of the seminal vesicle tissue response to acrylamide exposure. While we have yet to directly assess how RICTOR influences the physiological responses of seminal vesicle tissue, we found no evidence of overt modulation of either RICTOR expression of intracellular distribution in response to acrylamide challenge. Despite this, it is notable that deficiency of the closely related mTORC1 molecule regulatory-associated protein of MTOR complex 1 (RPTOR) does dysregulate seminal vesicle function (95), thus reinforcing the tenet that components of the mTOR complex play an important role in seminal vesicle biology. It is also notable that impaired mTORC2 signaling, mediated by RICTOR, has been implicated in increased cellular ROS sensitivity (96, 97).

The altered protein composition of seminal vesicle tissue following acrylamide exposure raises the question of whether seminal vesicle secretory function is similarly influenced. While no change in the weight of seminal vesicle tissue was detected, a decrease in seminal vesicle secretion volume and overall protein concentration was observed. This change in secretory function is consistent with other studies of epithelial cells in which environmental perturbations or genetic deficiency has been linked to a hyposecretory phenotype (98–100), yet the exact mechanisms by which this change is enacted remain uncertain. Additionally, our data implicates the synthesis of prominent seminal vesicle secreted factors, including SVS3A, SVS6, and PATE4, as being dysregulated in seminal vesicle tissue following acrylamide exposure. These proteins have well-established roles in copulatory plug formation (2, 9, 44), with PATE4-deficient male mice unable to form a complete copulatory plug leading to subfertility (9). Additional proteins with altered synthesis included the serine protease inhibitors SERPINA1D (101), SERPINA3K (102), and PLAU (103), which may contribute to copulatory plug formation, modification of sperm function, or activation of seminal fluid signaling molecules, as has been shown for other protease inhibitors in seminal fluid (104).

Taken together, these findings raise the possibility that alterations to seminal vesicle function may contribute to the embryonic loss observed following acute acrylamide exposure in the sire, as well as epididymal sperm changes (22, 69, 70). However, the specific proteomic impacts of acrylamide exposure on seminal vesicle fluid and the biological consequences of these changes remain to be addressed—particularly as this fluid constitutes a highly biased proteomic sample with a small subset of highly dominant proteins that rapidly coagulate upon recovery, making proteomic analysis and biological assessment of their functions challenging (42, 63). Indeed, our combined analysis of published seminal vesicle fluid proteomes (42–44) only identified 58 reviewed proteins from the UniProt database as being secreted by the seminal vesicle. These data further emphasize the importance of gaining a comprehensive profile of the true protein composition of seminal vesicle fluid, as acknowledged by Bayram *et al.*, (42). Our future studies aim to address this and increase the depth of the mouse seminal vesicle fluid proteome and explore the biological significance of altered seminal vesicle secretions on fertility and fetal development.

In summary, we have exploited an advanced proteomic platform to generate the first mechanistic insight into mouse seminal vesicles in normal physiology and pathology. These data identify how the seminal vesicle tissue responds to the reproductive toxicant, acrylamide, lending support to the emerging evidence that suggests we need to consider the responses of all male reproductive tract tissues when interpreting the potential impact of toxicants/environmental stressors on male fertility.

DATA AVAILABILITY

The mass spectrometry proteomics data have been deposited to the ProteomeXchange Consortium (http://proteomecentral.proteomexchange.org) *via* the PRIDE partner repository (105) with the dataset identifier PXD021998 and 10.6019/PXD021998.

Supplemental data—This article contains supplemental data (81, 82).

Acknowledgments—The authors gratefully acknowledge Nathan Smith from The University of Newcastle Analytical Biomolecular Research Facility (ABRF) and the Academic and Research Computing Support team at the University of Newcastle.

Funding and additional information—The preparation of this article was supported by the award of National Health and Medical Research Council (NHMRC) Project Grants APP1147932, awarded to B. N. and M. D. D., and APP1163319, awarded to B. N., R. J. A. and E. G. B. B. N. (APP1154837), M. D. D. (APP1173892), and E. G. B. (APP1138701) are recipients of NHMRC Research Fellowships.

Author contributions—D. A. S.-B., E. G. B., M. D. D., T. L., R. J. A., S. D. R., S. A. R., B. N., and J. E. S. conceptualization; D. A. S.-B. data curation; D. A. S.-B., I. R. B., A. L. A., S. J. S., L. A. M., and J. E. S. formal analysis; E. G. B., M. D. D., R. J. A., and B. N. funding acquisition; D. A. S.-B., N. A. T., and J. E. S. investigation; N. A. T., S. D. R., B. N., and J. E. S. methodology; B. N. and J. E. S. project administration; B. N. resources; S. A. R., B. N., and J. E. S. supervision; D. A. S.-B. and J. E. S. visualization; D. A. S.-B., I. R. B., A. L. A., S. J. S., and L. A. M. validation; D. A. S.-B., B. N., and J. E. S. writing—original draft; D. A. S.-B., N. A. T., E. G. B., M. D. D., I. R. B., A. L. A., S. J. S., L. A. M., T. L., R. J. A., S. D. R., S. A. R., B. N., and J. E. S. writing—review and editing.

Conflict of interest—The authors declare no conflicts of interest.

Abbreviations—The abbreviations used are: 8-OHdG, 8-hydroxy-2' -deoxyguanosine; αSMA, alpha smooth muscle actin; ARHGAP10, Rho GTPase-activating protein 10; B2M, Beta-2-microglobulin; BCAP29, B-cell receptor-associated protein 29; CAR1, carbonic anhydrase 2; CASP6, caspase-6; CD9, cluster of differentiation 9 antigen; CD38, ADP-ribosyl cyclase/cyclic ADP-ribose hydrolase 1; CDK4/6, cyclin-dependent kinase 4/6; CEACAM10, carcinoembryonic antigen-related cell adhesion molecule 10; DDA, Data-dependent acquisition; DKKL1, dickkopf-like protein 1; DNAJB5, DnaJ homolog subfamily B member 5; EIF2, eukaryotic initiation factor; EIF4EBP1, eukaryotic translation initiation factor 4E-binding protein 1; FDR, false discovery rate; HILIC, hydrophilic interaction liquid chromatography; HNRNPC, heterogeneous nuclear ribonucleoproteins C1/C2; IRAK4, interleukin-1 receptor-associated kinase 4; LARP1, La-related protein 1; LCN2, neutrophil gelatinase-associated lipocalin; LFQ, Label-free quantification; LIPA, lysosomal acid lipase/cholesteryl ester hydrolase; MFGE8, lactadherin; MLXIPL, MLX-interacting protein-like; MPZ, myelin protein P0; MSI2, RNA-binding protein Musashi homolog 2; MYC, Myc proto-oncogene protein; MYCN, N-myc proto-oncogene protein; nLC-MS/MS, nanoliquid chromatography–tandem mass spectrometry; NPC2, NPC intracellular cholesterol transporter 2; NRF2, nuclear factor erythroid 2-related factor-2; PATE4, prostate and testis expressed protein 4; PLAU, urokinase-type plasminogen activator; PSAP, prosaposin; QSOX1, sulfhydryl oxidase 1; RHO, Rho family of GTPases; RICTOR, rapamycin-insensitive companion of mTOR; RPL28, 60S ribosomal protein L28; SERPINA1D, alpha-1-antitrypsin 1–4; SERPINA3K, serine protease inhibitor A3K; SERPINE2, glia-derived nexin; SPINK1, serine protease inhibitor kazal-type 1; SPINKL, serine protease inhibitor kazal-like protein, minor form; SVS, seminal vesicle secretory protein; TBS, tris-buffered saline; TBST, TBS supplemented with 0.1% (v/v) Tween-20; TGM4, protein-glutamine gamma-glutamyltransferase 4; TP53, transcriptional regulator tumor protein p53; UGT1A7C, UDP-glucuronosyltransferase 1A7; V/V, percent volume/volume; W/V, percent weight/volume; WDR46, WD repeat-containing protein 46.

Received February 9, 2021, and in revised from, April 19, 2021
Published, MCPRO Papers in Press, June 2, 2021, https://doi.org/10.1016/j.mcpro.2021.100107

REFERENCES

1. Schjenken, J. E., Sharkey, D. J., and Robertson, S. A. (2018) Seminal vesicle—secretion. In: Skinner, M. K., ed. *Encyclopedia of Reproduction*, 2nd Ed, Academic Press, Oxford: 349–354
2. Noda, T., and Ikawa, M. (2019) Physiological function of seminal vesicle secretions on male fecundity. *Reprod. Med. Biol.* **18**, 241–246
3. Schjenken, J. E., and Robertson, S. A. (2020) The female response to seminal fluid. *Physiol. Rev.* **100**, 1077–1117
4. Bromfield, J. J., Ibrahim, L. A., and Rizo, J. A. (2018) Seminal vesicle gland—overview. In: Skinner, M. K., ed. *Encyclopedia of Reproduction*, 2nd Ed, Academic Press, Oxford: 341–343
5. Davies, D. C., Hall, G., Hibbitt, G., and Moore, H. D. (1975) The removal of the seminal vesicles from the boar and the effects on the semen characteristics. *J. Reprod. Fertil.* **43**, 305–312
6. Pang, S. F., Chow, P. H., and Wong, T. M. (1979) The role of the seminal vesicles, coagulating glands and prostate glands on the fertility and fecundity of mice. *J. Reprod. Fertil.* **56**, 129–132
7. Queen, K., Dhabuwala, C. B., and Pierrepoint, C. G. (1981) The effect of the removal of the various accessory sex glands on the fertility of male rats. *J. Reprod. Fertil.* **62**, 423–426
8. Kawano, N., Araki, N., Yoshida, K., Hibino, T., Ohnami, N., Makino, M., Kanai, S., Hasuwa, H., Yoshida, M., Miyado, K., and Umezawa, A. (2014) Seminal vesicle protein SVS2 is required for sperm survival in the uterus. *Proc. Natl. Acad. Sci. U. S. A.* **111**, 4145–4150
9. Noda, T., Fujihara, Y., Matsumura, T., Oura, S., Kobayashi, S., and Ikawa, M. (2019) Seminal vesicle secretory protein 7, PATE4, is not required for sperm function but for copulatory plug formation to ensure fecundity. *Biol. Reprod.* **100**, 1035–1045
10. Dean, M. D. (2013) Genetic disruption of the copulatory plug in mice leads to severely reduced fertility. *PLoS Genet.* **9**, e1003185
11. Kim, B. J., Park, D. R., Nam, T. S., Lee, S. H., and Kim, U. H. (2015) Seminal CD38 enhances human sperm capacitation through its interaction with CD31. *PLoS One* **10**, e0139110

12. Hess, E. A., Ludwick, T. M., Martig, R. C., and Ely, F. (1960) Influence of seminal vesiculectomy on certain physical and biochemical properties of bovine semen. *J. Dairy Sci.* **43**, 256–265
13. Ortiz, W. G., Rizo, J. A., Carvalheira, L. R., Ahmed, B. M. S., Estrada-Cortes, E., Harstine, B. R., Bromfield, J. J., and Hansen, P. J. (2019) Effects of intrauterine infusion of seminal plasma at artificial insemination on fertility of lactating Holstein cows. *J. Dairy Sci.* **102**, 6587–6594
14. Wong, C. L., Lee, K. H., Lo, K. M., Chan, O. C., Goggins, W., O, W. S., and Chow, P. H. (2007) Ablation of paternal accessory sex glands imparts physical and behavioural abnormalities to the progeny: An *in vivo* study in the golden hamster. *Theriogenology* **68**, 654–662
15. Morgan, H. L., and Watkins, A. J. (2020) The influence of seminal plasma on offspring development and health. *Semin. Cell Dev. Biol.* **97**, 131–137
16. Watkins, A. J., Dias, I., Tsuro, H., Allen, D., Emes, R. D., Moreton, J., Wilson, R., Ingram, R. J. M., and Sinclair, K. D. (2018) Paternal diet programs offspring health through sperm- and seminal plasma-specific pathways in mice. *Proc. Natl. Acad. Sci. U. S. A.* **115**, 10064–10069
17. Lane, M., Robker, R. L., and Robertson, S. A. (2014) Parenting from before conception. *Science* **345**, 756–760
18. Rocha, D. R., Martins, J. A., van Tilburg, M. F., Oliveira, R. V., Moreno, F. B., Monteiro-Moreira, A. C., Moreira, R. A., Araujo, A. A., and Moura, A. A. (2015) Effect of increased testicular temperature on seminal plasma proteome of the ram. *Theriogenology* **84**, 1291–1305
19. Li, Y., Hamilton, K. J., Wang, T., Coons, L. A., Jefferson, W. N., Li, R., Wang, Y., Grimm, S. A., Ramsey, J. T., Liu, L., Gerrish, K. E., Williams, C. J., Wade, P. A., and Korach, K. S. (2018) DNA methylation and transcriptome aberrations mediated by ERα in mouse seminal vesicles following developmental DES exposure. *Proc. Natl. Acad. Sci. U. S. A.* **115**, E4189–E4198
20. Binder, N. K., Sheedy, J. R., Hannan, N. J., and Gardner, D. K. (2015) Male obesity is associated with changed spermatozoa Cox4i1 mRNA level and altered seminal vesicle fluid composition in a mouse model. *Mol. Hum. Reprod.* **21**, 424–434
21. Bromfield, J. J., Schjenken, J. E., Chin, P. Y., Care, A. S., Jasper, M. J., and Robertson, S. A. (2014) Maternal tract factors contribute to paternal seminal fluid impact on metabolic phenotype in offspring. *Proc. Natl. Acad. Sci. U. S. A.* **111**, 2200–2205
22. Katen, A. L., Sipila, P., Mitchell, L. A., Stanger, S. J., Nixon, B., and Roman, S. D. (2017) Epididymal CYP2E1 plays a critical role in acrylamide-induced DNA damage in spermatozoa and paternally mediated embryonic resorptions. *Biol. Reprod.* **96**, 921–935
23. Katen, A. L., Chambers, C. G., Nixon, B., and Roman, S. D. (2016) Chronic acrylamide exposure in male mice results in elevated DNA damage in the germline and heritable induction of CYP2E1 in the testes. *Biol. Reprod.* **95**, 86
24. Nixon, B. J., Stanger, S. J., Nixon, B., and Roman, S. D. (2012) Chronic exposure to acrylamide induces DNA damage in male germ cells of mice. *Toxicol. Sci.* **129**, 135–145
25. Welsh, M., Moffat, L., Jack, L., McNeilly, A., Brownstein, D., Saunders, P. T., Sharpe, R. M., and Smith, L. B. (2010) Deletion of androgen receptor in the smooth muscle of the seminal vesicles impairs secretory function and alters its responsiveness to exogenous testosterone and estradiol. *Endocrinology* **151**, 3374–3385
26. Degryse, S., de Bock, C. E., Demeyer, S., Govaerts, I., Bornschein, S., Verbeke, D., Jacobs, K., Binos, S., Skerrett-Byrne, D. A., Murray, H. C., Verrills, N. M., Van Vlierberghe, P., Cools, J., and Dun, M. D. (2018) Mutant JAK3 phosphoproteomic profiling predicts synergism between JAK3 inhibitors and MEK/BCL2 inhibitors for the treatment of T-cell acute lymphoblastic leukemia. *Leukemia* **32**, 788–800
27. Nixon, B., De Iuliis, G. N., Hart, H. M., Zhou, W., Mathe, A., Bernstein, I. R., Anderson, A. L., Stanger, S. J., Skerrett-Byrne, D. A., Jamaluddin, M. F. B., Almazi, J. G., Bromfield, E. G., Larsen, M. R., and Dun, M. D. (2019) Proteomic profiling of mouse epididymosomes reveals their contributions to post-testicular sperm maturation. *Mol. Cell. Proteomics* **18**, S91–S108
28. Nixon, B., Johnston, S. D., Skerrett-Byrne, D. A., Anderson, A. L., Stanger, S. J., Bromfield, E. G., Martin, J. H., Hansbro, P. M., and Dun, M. D. (2019) Modification of crocodile spermatozoa refutes the tenet that post-testicular sperm maturation is restricted to mammals. *Mol. Cell. Proteomics* **18**, S59–S76
29. Dun, M. D., Chalkley, R. J., Faulkner, S., Keene, S., Avery-Kiejda, K. A., Scott, R. J., Falkenby, L. G., Cairns, M. J., Larsen, M. R., Bradshaw, R. A., and Hondermarck, H. (2015) Proteotranscriptomic profiling of 231-BR breast cancer cells: Identification of potential biomarkers and therapeutic targets for brain metastasis. *Mol. Cell. Proteomics* **14**, 2316–2330
30. Dun, M. D., Mannan, A., Rigby, C. J., Butler, S., Toop, H. D., Beck, D., Connerty, P., Sillar, J., Kahl, R. G. S., Duchatel, R. J., Germon, Z., Faulkner, S., Chi, M., Skerrett-Byrne, D., Murray, H. C., *et al*. (2020) Shwachman-Bodian-Diamond syndrome (SBDS) protein is a direct inhibitor of protein phosphatase 2A (PP2A) activity and overexpressed in acute myeloid leukaemia. *Leukemia* **34**, 3393–3397
31. Douse, C. H., Tchasovnikarova, I. A., Timms, R. T., Protasio, A. V., Seczynska, M., Prigozhin, D. M., Albecka, A., Wagstaff, J., Williamson, J. C., Freund, S. M. V., Lehner, P. J., and Modis, Y. (2020) TASOR is a pseudo-PARP that directs HUSH complex assembly and epigenetic transposon control. *Nat. Commun.* **11**, 4940
32. Lasch, P., Schneider, A., Blumenscheit, C., and Doellinger, J. (2020) Identification of microorganisms by liquid chromatography-mass spectrometry (LC-MS(1)) and in silico peptide mass libraries. *Mol. Cell. Proteomics* **19**, 2125–2138
33. Bruckbauer, S. T., Minkoff, B. B., Yu, D., Cryns, V. L., Cox, M. M., and Sussman, M. R. (2020) Ionizing radiation-induced proteomic oxidation in Escherichia coli. *Mol. Cell. Proteomics* **19**, 1375–1395
34. Hartel, N. G., Chew, B., Qin, J., Xu, J., and Graham, N. A. (2019) Deep protein methylation profiling by combined chemical and immunoaffinity approaches reveals novel PRMT1 targets. *Mol. Cell. Proteomics* **18**, 2149–2164
35. Federspiel, J. D., Greco, T. M., Lum, K. K., and Cristea, I. M. (2019) Hdac4 interactions in Huntington's disease viewed through the prism of multiomics. *Mol. Cell. Proteomics* **18**, S92–S113
36. Gomez-Herranz, M., Nekulova, M., Faktor, J., Hernychova, L., Kote, S., Sinclair, E. H., Nenutil, R., Vojtesek, B., Ball, K. L., and Hupp, T. R. (2019) The effects of IFITM1 and IFITM3 gene deletion on IFNgamma stimulated protein synthesis. *Cell Signal.* **60**, 39–56
37. Fasci, D., van Ingen, H., Scheltema, R. A., and Heck, A. J. R. (2018) Histone interaction landscapes visualized by crosslinking mass spectrometry in intact cell nuclei. *Mol. Cell. Proteomics* **17**, 2018–2033
38. Tyanova, S., Temu, T., Sinitcyn, P., Carlson, A., Hein, M. Y., Geiger, T., Mann, M., and Cox, J. (2016) The Perseus computational platform for comprehensive analysis of (prote)omics data. *Nat. Methods* **13**, 731–740
39. Krämer, A., Green, J., Pollard, J., Jr., and Tugendreich, S. (2014) Causal analysis approaches in ingenuity pathway analysis. *Bioinformatics* **30**, 523–530
40. Smith, C. L., and Eppig, J. T. (2009) The mammalian phenotype ontology: Enabling robust annotation and comparative analysis. *Wiley Interdiscip. Rev. Syst. Biol. Med.* **1**, 390–399
41. Dickinson, M. E., Flenniken, A. M., Ji, X., Teboul, L., Wong, M. D., White, J. K., Meehan, T. F., Weninger, W. J., Westerberg, H., Adissu, H., Baker, C. N., Bower, L., Brown, J. M., Caddle, L. B., Chiani, F., *et al*. (2016) High-throughput discovery of novel developmental phenotypes. *Nature* **537**, 508–514
42. Bayram, H. L., Franco, C., Brownridge, P., Claydon, A. J., Koch, N., Hurst, J. L., Beynon, R. J., and Stockley, P. (2020) Social status and ejaculate composition in the house mouse. *Philos. Trans. R. Soc. Lond. B Biol. Sci.* **375**, 20200083
43. Chang, W. C., Chou, C. K., Tsou, C. C., Li, S. H., Chen, C. H., Zhuo, Y. X., Hsu, W. L., and Chen, C. H. (2010) Comparative proteomic analysis of proteins involved in the tumorigenic process of seminal vesicle carcinoma in transgenic mice. *Int. J. Proteomics* **2010**, 726968
44. Dean, M. D., Clark, N. L., Findlay, G. D., Karn, R. C., Yi, X., Swanson, W. J., MacCoss, M. J., and Nachman, M. W. (2009) Proteomics and comparative genomic investigations reveal heterogeneity in evolutionary rate of male reproductive proteins in mice (Mus domesticus). *Mol. Biol. Evol.* **26**, 1733–1743
45. Schjenken, J. E., Moldenhauer, L. M., Zhang, B., Care, A. S., Groome, H. M., Chan, H. Y., Hope, C. M., Barry, S. C., and Robertson, S. A. (2020) MicroRNA miR-155 is required for expansion of regulatory T cells to mediate robust pregnancy tolerance in mice. *Mucosal Immunol.* **13**, 609–625
46. Schindelin, J., Arganda-Carreras, I., Frise, E., Kaynig, V., Longair, M., Pietzsch, T., Preibisch, S., Rueden, C., Saalfeld, S., Schmid, B.,

Tinevez, J.-Y., White, D. J., Hartenstein, V., Eliceiri, K., Tomancak, P., *et al*. (2012) Fiji: An open-source platform for biological-image analysis. *Nat. Methods* **9**, 676–682
47. Abràmoff, M. D., Magalhães, P. J., and Ram, S. J. (2004) Image processing with ImageJ. *Biophotonics Int.* **11**, 36–42
48. Houston, B. J., Nixon, B., Martin, J. H., De Iuliis, G. N., Trigg, N. A., Bromfield, E. G., McEwan, K. E., and Aitken, R. J. (2018) Heat exposure induces oxidative stress and DNA damage in the male germ line. *Biol. Reprod.* **98**, 593–606
49. Tremellen, K. P., Seamark, R. F., and Robertson, S. A. (1998) Seminal transforming growth factor beta1 stimulates granulocyte-macrophage colony-stimulating factor production and inflammatory cell recruitment in the murine uterus. *Biol. Reprod.* **58**, 1217–1225
50. Bennett, C. G., Riemondy, K., Chapnick, D. A., Bunker, E., Liu, X., Kuersten, S., and Yi, R. (2016) Genome-wide analysis of Musashi-2 targets reveals novel functions in governing epithelial cell migration. *Nucleic Acids Res.* **44**, 3788–3800
51. Ochiai, T., Takenaka, Y., Kuramoto, Y., Kasuya, M., Fukuda, K., Kimura, M., Shimeno, H., Misasi, R., Hiraiwa, M., and Soeda, S. (2008) Molecular mechanism for neuro-protective effect of prosaposin against oxidative stress: Its regulation of dimeric transcription factor formation. *Biochim. Biophys. Acta* **1780**, 1441–1447
52. Zhao, T., Ding, X., Du, H., and Yan, C. (2014) Myeloid-derived suppressor cells are involved in lysosomal acid lipase deficiency-induced endothelial cell dysfunctions. *J. Immunol.* **193**, 1942–1953
53. Brosseau, C., Colas, L., Magnan, A., and Brouard, S. (2018) CD9 tetraspanin: A new pathway for the regulation of inflammation? *Front. Immunol.* **9**, 2316
54. Adomavicius, T., Guaita, M., Zhou, Y., Jennings, M. D., Latif, Z., Roseman, A. M., and Pavitt, G. D. (2019) The structural basis of translational control by eIF2 phosphorylation. *Nat. Commun.* **10**, 2136
55. Lavrik, I., Golks, A., and Krammer, P. H. (2005) Death receptor signaling. *J. Cell Sci.* **118**, 265–267
56. Wang, X., and Proud, C. G. (2006) The mTOR pathway in the control of protein synthesis. *Physiology (Bethesda)* **21**, 362–369
57. Lamouille, S., Connolly, E., Smyth, J. W., Akhurst, R. J., and Derynck, R. (2012) TGF-beta-induced activation of mTOR complex 2 drives epithelial-mesenchymal transition and cell invasion. *J. Cell Sci.* **125**, 1259–1273
58. Sampson, L. L., Davis, A. K., Grogg, M. W., and Zheng, Y. (2016) mTOR disruption causes intestinal epithelial cell defects and intestinal atrophy postinjury in mice. *FASEB J.* **30**, 1263–1275
59. Katen, A. L., Stanger, S. J., Anderson, A. L., Nixon, B., and Roman, S. D. (2016) Chronic acrylamide exposure in male mice induces DNA damage to spermatozoa; potential for amelioration by resveratrol. *Reprod. Toxicol.* **63**, 1–12
60. Avivar-Valderas, A., Wen, H. C., and Aguirre-Ghiso, J. A. (2014) Stress signaling and the shaping of the mammary tissue in development and cancer. *Oncogene* **33**, 5483–5490
61. Delgado, M. E., Grabinger, T., and Brunner, T. (2016) Cell death at the intestinal epithelial front line. *FEBS J.* **283**, 2701–2719
62. Gudipaty, S. A., Conner, C. M., Rosenblatt, J., and Montell, D. J. (2018) Unconventional ways to live and die: Cell death and survival in development, homeostasis, and disease. *Annu. Rev. Cell Dev. Biol.* **34**, 311–332
63. Claydon, A. J., Ramm, S. A., Pennington, A., Hurst, J. L., Stockley, P., and Beynon, R. (2012) Heterogenous turnover of sperm and seminal vesicle proteins in the mouse revealed by dynamic metabolic labeling. *Mol. Cell. Proteomics* **11**. M111.014993
64. Ramm, S. A., Edward, D. A., Claydon, A. J., Hammond, D. E., Brownridge, P., Hurst, J. L., Beynon, R. J., and Stockley, P. (2015) Sperm competition risk drives plasticity in seminal fluid composition. *BMC Biol.* **13**, 87
65. Iamsaard, S., Tongpan, S., Yannasithinon, S., Arun, S., Wu, A. T. H., and Sukhorum, W. (2020) Effect of chronic stress on expression and secretion of seminal vesicle proteins in adult rats. *Andrologia* **53**, e13800
66. Kerwin, P., Yuan, J., and von Philipsborn, A. C. (2020) Female copulation song is modulated by seminal fluid. *Nat. Commun.* **11**, 1430
67. Weigmann, K. (2014) Lifestyle in the sperm: There is growing evidence that epigenetic marks can be inherited. But what is the nature of the information they store and over how many generations do they prevail? *EMBO Rep.* **15**, 1233–1237
68. JECFA. (2010) *Joint FAO/WHO Expert Committee on Food Additives. Summary Report of the Seventy-Second Meeting, Expert Committee on Food Additives*. Rome
69. Ghanayem, B. I., Witt, K. L., El-Hadri, L., Hoffler, U., Kissling, G. E., Shelby, M. D., and Bishop, J. B. (2005) Comparison of germ cell mutagenicity in male CYP2E1-null and wild-type mice treated with acrylamide: Evidence supporting a glycidamide-mediated effect. *Biol. Reprod.* **72**, 157–163
70. Shelby, M. D., Cain, K. T., Hughes, L. A., Braden, P. W., and Generoso, W. M. (1986) Dominant lethal effects of acrylamide in male mice. *Mutat. Res.* **173**, 35–40
71. Holland, N., Ahlborn, T., Turteltaub, K., Markee, C., Moore, D., 2nd, Wyrobek, A. J., and Smith, M. T. (1999) Acrylamide causes preimplantation abnormalities in embryos and induces chromatin-adducts in male germ cells of mice. *Reprod. Toxicol.* **13**, 167–178
72. Marchetti, F., Bishop, J., Lowe, X., and Wyrobek, A. J. (2009) Chromosomal mosaicism in mouse two-cell embryos after paternal exposure to acrylamide. *Toxicol. Sci.* **107**, 194–205
73. Koromilas, A. E. (2019) M(en)TORship lessons on life and death by the integrated stress response. *Biochim. Biophys. Acta Gen. Subj.* **1863**, 644–649
74. Tsounapi, P., Honda, M., Dimitriadis, F., Kawamoto, B., Hikita, K., Muraoka, K., Saito, M., Sofikitis, N., and Takenaka, A. (2017) Impact of antioxidants on seminal vesicles function and fertilizing potential in diabetic rats. *Asian J. Androl.* **19**, 639–646
75. Li, R., Li, H., Rao, K., Liu, K., Zhang, Y., Liu, X., Wang, T., Wang, S., Liu, Z., and Liu, J. (2019) Curcumin ameliorates atrophy of seminal vesicle via reduction of oxidative stress in castrated mice. *PeerJ* **7**, e7192
76. Hageman, J., van Waarde, M. A., Zylicz, A., Walerych, D., and Kampinga, H. H. (2011) The diverse members of the mammalian HSP70 machine show distinct chaperone-like activities. *Biochem. J.* **435**, 127–142
77. Ago, T., Liu, T., Zhai, P., Chen, W., Li, H., Molkentin, J. D., Vatner, S. F., and Sadoshima, J. (2008) A redox-dependent pathway for regulating class II HDACs and cardiac hypertrophy. *Cell* **133**, 978–993
78. Hageman, J., Rujano, M. A., van Waarde, M. A., Kakkar, V., Dirks, R. P., Govorukhina, N., Oosterveld-Hut, H. M., Lubsen, N. H., and Kampinga, H. H. (2010) A DNAJB chaperone subfamily with HDAC-dependent activities suppresses toxic protein aggregation. *Mol. Cell* **37**, 355–369
79. Tong, M., Chan, K. W., Bao, J. Y., Wong, K. Y., Chen, J. N., Kwan, P. S., Tang, K. H., Fu, L., Qin, Y. R., Lok, S., Guan, X. Y., and Ma, S. (2012) Rab25 is a tumor suppressor gene with antiangiogenic and anti-invasive activities in esophageal squamous cell carcinoma. *Cancer Res.* **72**, 6024–6035
80. Sims, A. C., Tilton, S. C., Menachery, V. D., Gralinski, L. E., Schäfer, A., Matzke, M. M., Webb-Robertson, B. J., Chang, J., Luna, M. L., Long, C. E., Shukla, A. K., Bankhead, A. R., 3rd, Burkett, S. E., Zornetzer, G., Tseng, C. T., *et al*. (2013) Release of severe acute respiratory syndrome coronavirus nuclear import block enhances host transcription in human lung cells. *J. Virol.* **87**, 3885–3902
81. Nagashima, D., Zhang, L., Kitamura, Y., Ichihara, S., Watanabe, E., Zong, C., Yamano, Y., Sakurai, T., Oikawa, S., and Ichihara, G. (2019) Proteomic analysis of hippocampal proteins in acrylamide-exposed Wistar rats. *Arch. Toxicol.* **93**, 1993–2006
82. Barber, D. S., Stevens, S., and LoPachin, R. M. (2007) Proteomic analysis of rat striatal synaptosomes during acrylamide intoxication at a low dose rate. *Toxicol. Sci.* **100**, 156–167
83. Simanainen, U., McNamara, K., Davey, R. A., Zajac, J. D., and Handelsman, D. J. (2008) Severe subfertility in mice with androgen receptor inactivation in sex accessory organs but not in testis. *Endocrinology* **149**, 3330–3338
84. Deanesly, R., and Parkes, A. S. (1933) Size changes in the seminal vesicles of the mouse during development and after castration. *J. Physiol.* **78**, 442–450
85. Camacho, L., Latendresse, J. R., Muskhelishvili, L., Patton, R., Bowyer, J. F., Thomas, M., and Doerge, D. R. (2012) Effects of acrylamide exposure on serum hormones, gene expression, cell proliferation, and histopathology in male reproductive tissues of Fischer 344 rats. *Toxicol. Lett.* **211**, 135–143
86. Anvari, M., Talebi, A. R., Mangoli, E., Shahedi, A., Ghasemi, M. R., and Pourentezari, M. (2020) Effects of acrylamide in the presence of vitamin

E on sperm parameters, chromatin quality, and testosterone levels in mice. *Clin. Exp. Reprod. Med.* **47**, 101–107
87. Bianco, J. J., Handelsman, D. J., Pedersen, J. S., and Risbridger, G. P. (2002) Direct response of the murine prostate gland and seminal vesicles to estradiol. *Endocrinology* **143**, 4922–4933
88. Robertson, S. A., Mau, V. J., Tremellen, K. P., and Seamark, R. F. (1996) Role of high molecular weight seminal vesicle proteins in eliciting the uterine inflammatory response to semen in mice. *J. Reprod. Fertil.* **107**, 265–277
89. Saxton, R. A., and Sabatini, D. M. (2017) mTOR signaling in growth, metabolism, and disease. *Cell* **168**, 960–976
90. Le Bacquer, O., Queniat, G., Gmyr, V., Kerr-Conte, J., Lefebvre, B., and Pattou, F. (2013) mTORC1 and mTORC2 regulate insulin secretion through Akt in INS-1 cells. *J. Endocrinol.* **216**, 21–29
91. Morrison, M. M., Young, C. D., Wang, S., Sobolik, T., Sanchez, V. M., Hicks, D. J., Cook, R. S., and Brantley-Sieders, D. M. (2015) mTOR directs breast morphogenesis through the PKC-alpha-Rac1 signaling axis. *PLoS Genet.* **11**, e1005291
92. Jankiewicz, M., Groner, B., and Desrivières, S. (2006) Mammalian target of Rapamycin regulates the growth of mammary epithelial cells through the inhibitor of deoxyribonucleic acid binding Id1 and their functional differentiation through Id2. *Mol. Endocrinol.* **20**, 2369–2381
93. Pauloin, A., and Chanat, E. (2012) Prolactin and epidermal growth factor stimulate adipophilin synthesis in HC11 mouse mammary epithelial cells via the PI3-kinase/Akt/mTOR pathway. *Biochim. Biophys. Acta* **1823**, 987–996
94. Serrano, I., McDonald, P. C., Lock, F. E., and Dedhar, S. (2013) Role of the integrin-linked kinase (ILK)/Rictor complex in TGFbeta-1-induced epithelial-mesenchymal transition (EMT). *Oncogene* **32**, 50–60
95. Schell, C., Kretz, O., Liang, W., Kiefer, B., Schneider, S., Sellung, D., Bork, T., Leiber, C., Rüegg, M. A., Mallidis, C., Schlatt, S., Mayerhofer, A., Huber, T. B., and Grahammer, F. (2016) The rapamycin-sensitive complex of mammalian target of Rapamycin is essential to maintain male fertility. *Am. J. Pathol.* **186**, 324–336
96. Cai, W., and Andres, D. A. (2014) mTORC2 is required for rit-mediated oxidative stress resistance. *PLoS One* **9**, e115602
97. Wang, R.-H., Kim, H.-S., Xiao, C., Xu, X., Gavrilova, O., and Deng, C.-X. (2011) Hepatic Sirt1 deficiency in mice impairs mTorc2/Akt signaling and results in hyperglycemia, oxidative damage, and insulin resistance. *J. Clin. Invest.* **121**, 4477–4490
98. Yang, H. S., Sim, H. J., Cho, H., Bang, W. Y., Kim, H. E., Kwon, T. K., Kwon, T., and Park, T. J. (2020) Alpha-tocopherol exerts protective function against the mucotoxicity of particulate matter in amphibian and human goblet cells. *Sci. Rep.* **10**, 6224
99. Kim, S. C., Lee, H. J., Joo, J. H., Yoon, J. H., and Choi, J. Y. (2012) Vitamin A deficiency induces fluid hyposecretion from the airway submucosal glands of mice. *J. Nutr.* **142**, 739–743
100. Shea-Donohue, T., Notari, L., Stiltz, J., Sun, R., Madden, K. B., Urban, J. F., Jr., and Zhao, A. (2010) Role of enteric nerves in immune-mediated changes in protease-activated receptor 2 effects on gut function. *Neurogastroenterol. Motil.* **22**, e1138–e1291
101. Winkler, I. G., Hendy, J., Coughlin, P., Horvath, A., and Levesque, J. P. (2005) Serine protease inhibitors serpina1 and serpina3 are down-regulated in bone marrow during hematopoietic progenitor mobilization. *J. Exp. Med.* **201**, 1077–1088
102. Takahara, H., and Sinohara, H. (1982) Mouse plasma trypsin inhibitors: Inhibitory spectrum of contrapsin and alpha-1-antitrypsin. *Thromb. Res.* **27**, 45–50
103. Vassalli, J.-D., Huarte, J., Bosco, D., Sappino, A.-P., Sappino, N., Velardi, A., Wohlwend, A., Ernø, H., Monard, D., and Belin, D. (1993) Protease-nexin I as an androgen-dependent secretory product of the murine seminal vesicle. *EMBO J.* **12**, 1871–1878
104. Laflamme, B. A., and Wolfner, M. F. (2013) Identification and function of proteolysis regulators in seminal fluid. *Mol. Reprod. Dev.* **80**, 80–101
105. Perez-Riverol, Y., Csordas, A., Bai, J., Bernal-Llinares, M., Hewapathirana, S., Kundu, D. J., Inuganti, A., Griss, J., Mayer, G., Eisenacher, M., Perez, E., Uszkoreit, J., Pfeuffer, J., Sachsenberg, T., Yilmaz, S., *et al*. (2019) The PRIDE database and related tools and resources in 2019: Improving support for quantification data. *Nucleic Acids Res.* **47**, D442–D450